IEEE Access
Multidisciplinary ⋮ Rapid Review ⋮ Open Access Journal

Received May 30, 2021, accepted June 10, 2021, date of publication June 14, 2021, date of current version June 22, 2021.

Digital Object Identifier 10.1109/ACCESS.2021.3088997

The Evolution of Faster-Than-Nyquist Signaling

TAKUMI ISHIHARA[1], (Member, IEEE), SHINYA SUGIURA[1], (Senior Member, IEEE), AND LAJOS HANZO[2], (Fellow, IEEE)

[1]Institute of Industrial Science, The University of Tokyo, Tokyo 153-8505, Japan
[2]Department of Electronics and Computer Science, University of Southampton, Southampton SO17 1BJ, U.K.

Corresponding author: Lajos Hanzo (lh@ecs.soton.ac.uk)

The work of Takumi Ishihara was supported in part by the Japan Society for the Promotion of Science (JSPS) KAKENHI under Grant 20K22410. The work of Shinya Sugiura was supported in part by the JSPS KAKENHI under Grant 16KK0120, Grant 17H03259, and Grant 17K18871; and in part by Japan Science and Technology Agency (JST) Precursory Research for Embryonic Science and Technology (PRESTO) under Grant JPMJPR1933. The work of Lajos Hanzo was supported in part by the Engineering and Physical Sciences Research Council under Project EP/P034284/1 and Project EP/P003990/1 (COALESCE) and in part by the European Research Council's Advanced Fellow Grant QuantCom under Grant 789028.

ABSTRACT The fifty-year progress of faster-than-Nyquist (FTN) signaling is surveyed. FTN signaling exploits non-orthogonal dense symbol packing in the time domain for the sake of increasing the data rate attained. After reviewing the system models of both the conventional Nyquist-based and FTN signaling transceivers, we survey the evolution of FTN techniques, including their low-complexity detection and channel estimation. Furthermore, in addition to the classic FTN signaling philosophy, we introduce the recent frequency-domain filtering and precoding aided schemes. When relying on precoding, the information rate of FTN signaling becomes related to the eigenvalues of an FTN-specific intersymbol interference matrix, which provides a unified framework for the associated information-theoretic analysis and simplifies the associated power allocation specifically designed for increasing the information rate attained. We show that the FTN signaling scheme combined with bespoke power allocation employing a realistic raised-cosine shaping filter achieves the Shannon capacity associated with ideal rectangular shaping filters.

INDEX TERMS Capacity, detection, faster-than-Nyquist signaling, interference, precoding.

I. INTRODUCTION

Since the 1960s [1]–[3], faster-than-Nyquist (FTN) signaling has attracted researchers in the field of communications, owing to its potential of increasing the information rate beyond the bound defined by the classic Nyquist criterion. Most of the existing wireless standards follow the Nyquist criterion, hence facilitating interference-free symbol-by-symbol detection at the receiver in a frequency-flat channel. Classically, Shannon's capacity was derived under the assumption of orthogonal signaling based on the Nyquist criterion relying on the employment of an ideal rectangular shaping filter [4]. In contrast to Nyquist signaling, FTN signaling relies on the transmission of non-orthogonal pulses in the time domain. In FTN signaling, the signaling pulses have a symbol interval T shorter than that defined by the Nyquist criterion, i.e., $T = \tau T_0$, where T_0 represents the Nyquist-criterion-based ISI-free minimum symbol interval and the coefficient τ $(0 < \tau \leq 1)$ denotes the symbol packing ratio. Naturally, the potential bitrate increase of FTN signaling is achieved at the cost of unavoidable inter-symbol interference (ISI) effects even in a frequency-flat channel.

Most of the studies of FTN signaling can be classified into four categories: information-theoretic analysis [5]–[18], reduced-complexity receiver [19]–[40], channel estimation (CE) issues [35], [39], [41]–[43], and transmit preprocessing/precoding [13]–[15], [18], [21], [44]–[51]. In the information-theoretic studies, the achievable performance gains of FTN signaling over Nyquist signaling were investigated in terms of several metrics, such as the minimum Euclidean distance (MED), the mutual information, the capacity and the bit error ratio (BER). Until recently, most of the information-theoretic studies were conducted for simple FTN signaling architectures dispensing with precoding.

Attractive reduced-complexity detection schemes have been developed for FTN signaling operating both in the time-domain (TD) [19]–[29] and frequency-domain (FD) [30]–[40], in order to combat the fundamental limitations imposed by the FTN-specific ISI effects. Following the invention of powerful near-capacity channel coding schemes [53], such as turbo and low-density parity-check (LDPC) coding, typically channel-encoded schemes

The associate editor coordinating the review of this manuscript and approving it for publication was Pietro Savazzi.

TABLE 1. Surveys and tutorials on Faster-than-Nyquist signaling.

	Publication year	Dates back to	FTN transceiver design			CE issues	Information-theoretic analysis	
			TD	FD	Precoded		Unprecoded	Precoded
Anderson *et al.* [4]	2013	1975	✓				✓	
Fan *et al.* [52]	2017	1975	✓	✓		✓	✓	
This treatise		1965	✓	✓	✓	✓	✓	✓

have been used for eliminating the ISI effects in FTN signaling systems. The optimal maximum likelihood sequence estimator (MLSE) is too complex for demodulating/decoding the ISI-contaminated FTN symbols. Thus, the development of reduced-complexity detection has been one of the main issues in FTN signaling studies [4], [52]. Since the received signal model of FTN signaling is formulated as a block-based representation, similar to code-division multiple-access (CDMA) and multiple-input multiple-output (MIMO) systems [54], many of the efficient detection algorithms originally developed for CDMA and MIMO systems have been appropriately adapted for FTN signaling receivers. Moreover, similar to other wireless communication schemes, accurate CE is of pivotal importance for FTN signaling, where the channels are typically estimated by using pilot symbols inserted into a data frame [35], [39], [41]–[43]. Then, the estimated channel coefficients are used for demodulating the information symbols, and hence the accuracy of CE critically affects the achievable performance.

More recently, transmit precoding (TPC) schemes have been extensively investigated in the context of FTN signaling [13]–[15], [18], [21], [44]–[49]. The design objectives of the TPC schemes include increasing the MED and eliminating the ISI effects; these schemes operate either at the transmitter or jointly at both the transmitter and receiver. Furthermore, with the aid of the recent eigendecomposition-based TPC [14], [15], [18], [44], it becomes possible to consider an ISI-free received signal model having parallel substreams. This allows us to formulate the information-theoretic analysis of FTN signaling in a simplified manner and obtain novel additional insights beyond those emerging from the early FTN studies.

Bearing the above history in mind, we provide an accessible survey and tutorial on FTN signaling. The novel contributions of this treatise are as follows:

- After introducing the system models of the conventional Nyquist- and FTN-signaling based transceivers, the low-complexity TD and FD FTN detection schemes are reviewed. Moreover, CE and noncoherent detection of FTN signaling are presented. The novel contributions of this treatise over the pair of existing survey papers [4], [52] are summarized in Table 1.
- In addition to the classic unprecoded FTN signaling schemes, we introduce the recent FD filtering and TPC schemes while formulating the associated analytical framework.
- Furthermore, we provide comprehensive comparisons of the information rate achievable by FTN signaling and the gain over the classic Nyquist-based signaling, employing a realistic root RC (RRC) shaping filter.

The remainder of this paper is organized as follows. In Section II, we revisit the system model of the classic Nyquist signaling transceiver model, while in Section III the conventional unprecoded FTN signaling architecture is introduced. Then, in Sections IV and V, we review the family of low-complexity detection algorithms operating in the TD and FD, respectively. In Section VI, CE issues are discussed. In Section VII, the recent advances of the precoded FTN signaling family are detailed, while in Section VIII, its information-theoretic analysis is provided. Section IX summarizes the additional related studies. Finally, this paper is concluded in Section X with a discussion of future research directions. The structure of this treatise is shown in Fig. 1.

II. CLASSIC NYQUIST-CRITERION-BASED SIGNALING

In this section, we briefly review the conventional bandlimited orthogonal signaling scheme based on the time-orthogonal Nyquist criterion.

A. SYSTEM MODEL

Let us consider baseband signals of the form:

$$s(t) = \sum_n s_n q(t - nT_0), \tag{1}$$

where $s_n \in \mathbb{C}$ represents the nth complex-valued information symbol, and $q(t)$ is the impulse response (IR) of a shaping filter. Each symbol is passed through $q(t)$ with a symbol interval of T_0. The signal $s(t)$ is then transmitted to the receiver over a channel.

Under the assumption of an additive white Gaussian noise (AWGN) channel, the received signals $y(t) \in \mathbb{C}$ after matched filtering are given by

$$y(t) = \sum_n s_n g(t - nT_0) + \eta(t), \tag{2}$$

where we have

$$g(t) = \int q(\xi) q^*(\xi - t) d\xi \tag{3}$$

$$\eta(t) = \int n(\xi) q^*(\xi - t) d\xi. \tag{4}$$

In (4), $n(t)$ represents noise signals obeying the zero-mean complex-valued Gaussian distribution of $\mathcal{CN}(0, N_0)$, which has a variance of N_0. Then, the symbol $y_k = y(kT_0)$ sampled at the kth interval is represented by [55]

$$y_k = \sum_n s_n g((k - n)T_0) + \eta(kT_0) \tag{5}$$

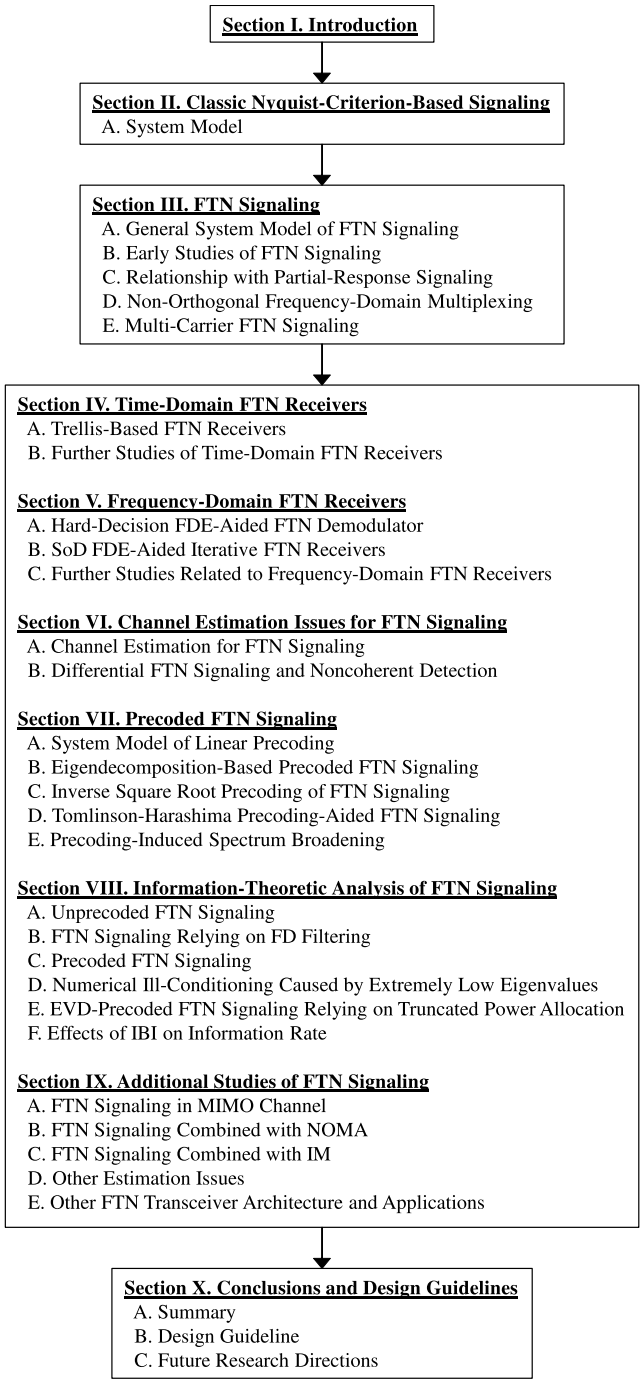

FIGURE 1. Structure of this treatise.

$$= s_k g(0) + \sum_{n \neq k} s_n g((k-n)T_0) + \eta(kT_0). \tag{6}$$

The first term of (6) represents the symbol of interest, while the second term corresponds to the ISI components.

In order to avoid ISI, the second term of (6) has to be zero. This imposes the condition of time-orthogonality on the shaping pulse $g(t)$ formulated as follows [55], [56]:

$$g(kT_0) = \begin{cases} 1, & \text{for } k = 0 \\ 0, & \text{for } k \neq 0, \end{cases} \tag{7}$$

where $g(t)$ is normalized for ensuring that $g(0) = 1$, and (7) is referred to as the *Nyquist criterion* or *Nyquist condition for zero ISI* [55], [56].

If we define $H(f)$ as the frequency response of $g(t)$, then $g(t)$ is given by $g(t) = \int_{-\infty}^{\infty} H(f) e^{j2\pi ft}$. Hence, (7) can be rewritten as [55]

$$g(kT_0) = \int_{-\infty}^{\infty} H(f) e^{j2\pi fkT_0} df \tag{8}$$

$$= \sum_{m=-\infty}^{\infty} \int_{(2m-1)/2T_0}^{(2m+1)/2T_0} H(f) e^{j2\pi fkT_0} df \tag{9}$$

$$= \int_{-1/2T_0}^{1/2T_0} \left\{ \sum_{m=-\infty}^{\infty} H\left(f + \frac{m}{T_0}\right) \right\} e^{j2\pi fkT_0} df \tag{10}$$

$$= \int_{-1/2T_0}^{1/2T_0} X(f) e^{j2\pi fkT_0} df, \tag{11}$$

where $X(f) = \sum_{m=-\infty}^{\infty} H(f + m/T_0)$. Since $X(f)$ is a periodic function having the period $1/T_0$, the Fourier series expansion of $X(f)$ is given by [55]

$$X(f) = \sum_{k=-\infty}^{\infty} c_k e^{j2\pi kfT_0}, \tag{12}$$

where c_k represent the Fourier series coefficients of $X(f)$, which are calculated by

$$c_k = T_0 \int_{-1/2T_0}^{1/2T_0} X(f) e^{-j2\pi kfT_0} df \tag{13}$$

$$= T_0 g(-kT_0) \tag{14}$$

$$= \begin{cases} T_0, & \text{for } k = 0 \\ 0, & \text{for } k \neq 0 \end{cases} \tag{15}$$

Hence, from (12) and (15), we arrive at the Nyquist criterion in the FD as follows [55], [56]:

$$\sum_{m=-\infty}^{\infty} H\left(f + \frac{m}{T_0}\right) = T_0. \tag{16}$$

This indicates that in order to avoid ISI, the sum of shifted frequency responses $H(f + m/T_0)$ has to be a constant value of T_0.

Fig. 2 shows a typical spectrum pattern of $X(f)$, where the communication channel is strictly bandlimited within the frequency range of $[-W, W]$ and W [Hz] is the one-sided bandwidth. More specifically, Figs. 2(a), 2(b), and 2(c) show the three scenarios of $T_0 = 1/(2W)$, $T_0 > 1/(2W)$, and $T_0 < 1/(2W)$, respectively [55]. Observe in Fig. 2(a) that for $T_0 = 1/(2W)$, the shifted frequency responses $H(f + m/T_0)$ do not overlap each other and the rectangular frequency response having the bandwidth of $2W$ is the unique solution that satisfies the Nyquist criterion of (16), which is given by [55], [56]

$$H(f) = \begin{cases} T_0 & \text{for } -W \leq f \leq W \\ 0, & \text{for } |f| > W. \end{cases} \tag{17}$$

Note also that the TD function corresponding to (17) is given by a sinc pulse $\sin(\pi t/T_0)/(\pi t/T_0)$. Additionally, for

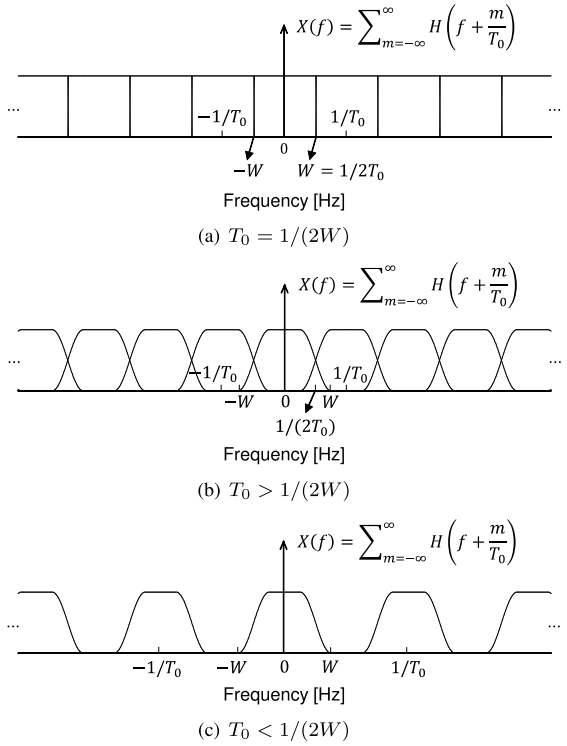

FIGURE 2. Spectrum patterns $X(f) = \sum_{m=-\infty}^{\infty} H(f + m/T_0)$ under the assumption of strictly limited bandwidth within $[-W, W]$.

the $T_0 > 1/(2W)$ scenario of Fig. 2(b), diverse frequency characteristics that satisfy the Nyquist criterion (16) are conceivable [55], while for the $T_0 < 1/(2W)$ scenario of Fig. 2(c), there exists no pulse shape that satisfies the Nyquist criterion (16) due to the presence of spectral nulls in $X(f)$, which induce unavoidable ISI.

According to the above discussion, in a bandlimited communication channel having a bandwidth of $2W$, the Nyquist criterion (16) is satisfied when the symbol interval is set to $T_0 \geq 1/(2W)$. Thus, the ISI-free minimum symbol interval is defined by $T_0 = 1/(2W)$. By contrast, for the scenario of $T_0 < 1/(2W)$, which corresponds to FTN signaling [1]–[3], the transmission symbol rate becomes higher than the $1/T_0 = 2W$ value defined by the Nyquist criterion at the cost of introducing ISI.

Although the use of the rectangular filter of (17) allows the ISI-free maximum symbol rate in a bandlimited channel, it is a challenging task to implement an ideal sinc pulse [4], [56]. To circumvent this limitation, typically a raised-cosine (RC) shaping filter is employed [55], [56]. The FD and TD characteristics of an RC shaping filter are defined by [55]

$$H_{\mathrm{RC}}(f) = \begin{cases} T_0 & |f| \leq \dfrac{1-\beta}{2T_0} \\ 0 & |f| > \dfrac{1+\beta}{2T_0} \\ \dfrac{T_0}{2}\left[1+\cos\left\{\dfrac{\pi T_0}{\beta}\left(|f|-\dfrac{1-\beta}{2T_0}\right)\right\}\right] & \text{otherwise,} \end{cases} \tag{18}$$

and

$$g(t) = \mathrm{sinc}\left(\frac{t}{T_0}\right)\frac{\cos\left(\frac{\beta\pi t}{T_0}\right)}{1-4\left(\frac{\beta t}{T_0}\right)^2}, \tag{19}$$

respectively, where the relationship $T_0 = 1/(2W)$ holds. Moreover, the bandwidth of an RC shaping filter is given by $2(1+\beta)W$, where β denotes a roll-off factor that determines the amount of excess bandwidth. The RC shaping filter having a roll-off factor of $\beta = 0$ corresponds to the rectangular shaping filter.

Furthermore, in order to allow the employment of identical shaping filters at the transmitter and the receiver, while satisfying the Nyquist criterion, an RRC shaping filter, having a frequency response of $H_{\mathrm{RRC}}(f) = \sqrt{H_{\mathrm{RC}}(f)}$, is typically employed. The TD pulse shape of an RRC filter having a roll-off factor β is given by [57]

$$q(t) = \begin{cases} \dfrac{1}{\sqrt{T_0}}\left(1-\beta+\dfrac{4\beta}{\pi}\right) & \text{for } t = 0 \\ \dfrac{\beta}{\sqrt{2T_0}}\left\{\left(1+\dfrac{2}{\pi}\right)\sin\left(\dfrac{\pi}{4\beta}\right) + \left(1-\dfrac{2}{\pi}\right)\cos\left(\dfrac{\pi}{4\beta}\right)\right\} & \text{for } t = \pm\dfrac{T_0}{4\beta} \\ \dfrac{\sin\left(\frac{t\pi}{T_0}(1-\beta)\right)+\frac{4\beta t}{T_0}\cos\left(\frac{\pi t}{T_0}(1+\beta)\right)}{\frac{\pi t}{\sqrt{T_0}}\left\{1-\left(\frac{4\beta t}{T_0}\right)^2\right\}} & \text{otherwise,} \end{cases} \tag{20}$$

where $q(t)$ has a unit-energy of $\int_{-\infty}^{\infty}|q(t)|^2 dt = 1$ [57].

III. FTN SIGNALING

In Section II, we reviewed the classic Nyquist criterion, which has been typically employed in conventional communication systems for reliable ISI-free information transmission. In contrast to classic Nyquist signaling whose maximum symbol rate is $1/T_0 = 2W$, the concept of FTN signaling has been conceived for attaining a symbol rate higher than $1/T_0$. In this section, we introduce the general system model of FTN signaling and review the early studies.

A. GENERAL SYSTEM MODEL OF FTN SIGNALING

Fig. 3 shows the uncoded FTN transceiver architecture. At the transmitter, using phase-shift keying (PSK) and quadrature amplitude modulation (QAM), a B-length information bits $\mathbf{b} = [b_0, b_1, \cdots, b_{B-1}] \in \mathbb{Z}^B$ are mapped onto an N-length complex-valued symbols $\mathbf{s} = [s_0, s_1, \cdots, s_{N-1}]^T \in \mathbb{C}^N$, which have $\mathbb{E}[|s_k|^2] = \sigma_s^2$ $(n = 0, \cdots, N-1)$, where $\mathbb{E}[\cdot]$ denotes the expectation operation. Then, the N-symbols vector $\mathbf{s}$ is passed through the RRC shaping filter having a roll-off factor of β. The symbol interval is set to $T = \tau T_0$ $(0 < \tau \leq 1)$, which is lower than the ISI-free minimum symbol interval T_0 defined by the Nyquist criterion. Hence, FTN signaling may achieve a higher symbol rate

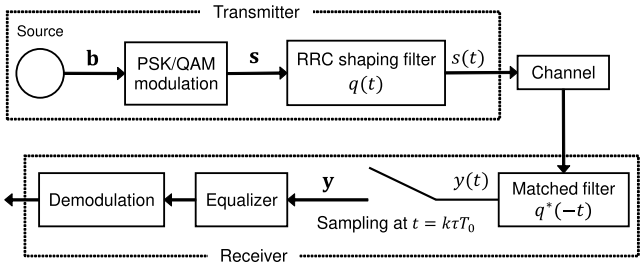

FIGURE 3. Uncoded FTN signaling transceiver architecture.

than the conventional Nyquist-criterion-based upper bound, at the cost of introducing ISI. The coefficient τ represents the symbol packing ratio, where a low τ corresponds to a high FTN signaling rate. In general, the detrimental effects of an FTN-specific ISI tend to increase upon reducing the symbol packing ratio τ. The baseband FTN signals are given by

$$s(t) = \sum_{n=0}^{N-1} s_n q(t - nT). \tag{21}$$

The FTN signaling scheme hence sends $1/\tau$ times more symbols per second than its conventional Nyquist signaling counterpart. The average transmit energy E_N of an N-length FTN signaling block $s(t)$ is given by

$$\begin{aligned} E_N &= \mathbb{E}\left[\int_{-\infty}^{\infty} |s(t)|^2 dt\right] && (22)\\ &= \mathbb{E}\left[\int_{-\infty}^{\infty} \sum_{l=0}^{N-1}\sum_{m=0}^{N-1} s_l s_m^* q(t - lT) q^*(t - mT) dt\right] && (23)\\ &= \mathbb{E}\left[\sum_{l=0}^{N-1}\sum_{m=0}^{N-1} s_l s_m^* g((m-l)T)\right] && (24)\\ &= \sum_{n=0}^{N-1}\left\{\mathbb{E}\left[|s_n|^2\right] g(0)\right\} && (25)\\ &= N\sigma_s^2, && (26) \end{aligned}$$

where we have $\int_{-\infty}^{\infty} q(t - lT)q^*(t - mT)dt = g((m - l)T)$. Moreover, $\mathbb{E}[s_l s_m^*] = 0$ for $l \neq m$ and $g(0) = 1$.

The received signal is then matched-filtered with the aid of $q^*(-t)$ to obtain

$$y(t) = \sum_n s_n g(t - nT) + \eta(t), \tag{27}$$

where $g(t)$ and $\eta(t)$ are given by (3) and (4), respectively.

Then, the matched-filtered signal (27) is sampled at the FTN-specific symbol interval $T = \tau T_0$, where the kth sample is represented by

$$\begin{aligned} y_k &= y(kT) && (28)\\ &= \sum_n s_n g((k-n)T) + \eta(kT). && (29) \end{aligned}$$

Furthermore, (29) is rewritten in form of its block-based representation, given its received sample block $\mathbf{y} = [y_0, y_1, \cdots, y_{N-1}]^T \in \mathbb{C}^N$ as follows:

$$\mathbf{y} = \mathbf{G}\mathbf{s} + \boldsymbol{\eta}, \tag{30}$$

where the matrix $\mathbf{G} \in \mathbb{R}^{N\times N}$ represents the FTN-induced ISI, which is given by

$$\mathbf{G} = \begin{bmatrix} g(0) & g(-T) & \cdots & g(-(N-1)T) \\ g(T) & g(0) & \cdots & g(-(N-2)T) \\ g(2T) & g(T) & \cdots & g(-(N-3)T) \\ \vdots & \vdots & \ddots & \vdots \\ g((N-1)T) & g((N-2)T) & \cdots & g(0) \end{bmatrix}. \tag{31}$$

Furthermore, $\boldsymbol{\eta} = [\eta(0), \eta(T), \cdots, \eta((N-1)T)]^T \in \mathbb{C}^N$ in (30) denotes the associated noise samples, which have a correlation matrix of

$$\mathbb{E}\left[\boldsymbol{\eta}\boldsymbol{\eta}^H\right] = N_0\mathbf{G}. \tag{32}$$

Note that in the classic Nyquist signaling, which corresponds to the scenario of $\tau = 1$, the matrix $\mathbf{G}$ becomes the $(N \times N)$-element identity matrix $\mathbf{I}_N$, and hence no ISI or noise correlation is imposed. Fig. 4 shows the waveforms of Nyquist signaling and FTN signaling, each employing an RC shaping filter with the roll-off factor of $\beta = 0.25$. The symbol packing ratio of $\tau = 0.8$ was set for FTN signaling. The transmission of the binary PSK (BPSK) symbol vector of $[1, -1, 1, -1, 1, 1]$ was considered. While in Nyquist signaling no ISI was encountered at each symbol timing of $t = nT_0$ $(n = 0, 1, \cdots, 5)$, in FTN signaling detrimental ISI was encountered at each FTN symbol timing of $t = n\tau T_0$, while achieving a higher symbol rate than its Nyquist signaling counterpart.

Moreover, in an L-tap frequency-selective fading channel having the channel coefficients of h_l $(l = 0, 1, \cdots, L-1)$, the received FTN signals, corresponding to (27), are given by [30], [35], [39]

$$y(t) = \sum_{l=0}^{L-1}\sum_n h_l s_n g(t - (l+n)T) + \eta(t). \tag{33}$$

The received sample block $\mathbf{y} = [y(0), y(T), \cdots, y((N-1)T)]^T \in \mathbb{C}^N$ is represented by

$$\mathbf{y} = \mathbf{G}_h\mathbf{s} + \boldsymbol{\eta}, \tag{34}$$

where the ath row and bth column entry of the ISI matrix $\mathbf{G}_h \in \mathbb{C}^{N\times N}$ is given by

$$\mathbf{G}_h(a, b) = \sum_{l=0}^{L-1} h_l g(aT - (b+l)T). \tag{35}$$

B. EARLY STUDIES OF FTN SIGNALING

In the following, we review the early studies of the FTN signaling concept [1]–[3], [58]–[67]. The seminal treatises and their specific contributions are listed in Table 2.

TABLE 2. Key works of FTN signaling and their contributions.

Year	Authors	Contribution
1965	Tufts [1]	Proposed FTN signaling for the first time, while considering a simplified model supporting nine to eleven overlapped PAM-aided symbols per block.
1968	Saltzberg [2]	Showed a 3% bandwidth-efficiency gain of FTN signaling over Nyquist signaling in an ideal noise-less channel.
1970	Lucky [58]	Introduced the DFE algorithm for FTN signaling.
1973	Salz [59]	Proposed the MMSE-based DFE algorithm for FTN signaling.
1975	Mazo [3]	Investigated the MED of FTN signaling with the aid of the ideal sinc filter, revealing that if symbol packing ratio τ is higher than 0.802, then the MED of FTN signaling is the same as that of Nyquist signaling.
1984	Foschini [60]	Proposed a shaping filter that maximizes the MED of binary FTN signaling, which achieved a slight performance gain over Nyquist signaling.
1987	Fihel and Sari [61]	Proposed the 16-QAM-aided FTN signaling scheme as an alternative to its 64-QAM-aided Nyquist signaling counterpart.
1995	Wang and Lee [62]	Proposed a precoding scheme to maximize the MED based on the error sequence of two different FTN signaling codewords.

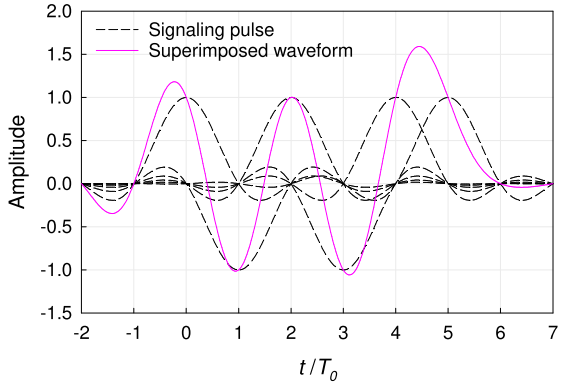

(a) Nyquist signaling.

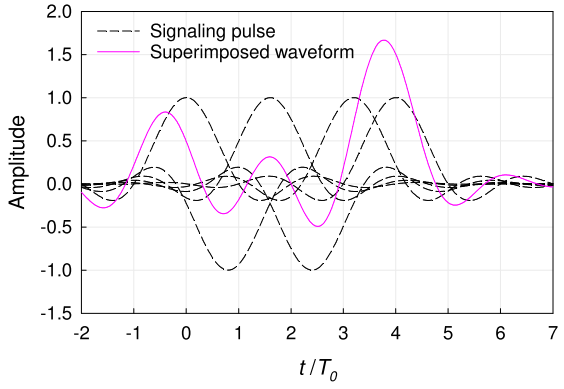

(b) FTN signaling with $\tau = 0.8$.

FIGURE 4. Exemplifying the waveform of (a) Nyquist signaling and (b) FTN signaling. The use of an RC shaping filter having the roll-off factor of $\beta = 0.25$ was considered. The symbol packing ratio of FTN signaling was set to $\tau = 0.8$.

1) ESTABLISHMENT OF THE FTN SIGNALING CONCEPT

The concept of FTN signaling was established in the earliest studies of [1], [2], [58], [59]. In [1], Tufts proposed FTN signaling and a least mean square error (MSE) receiver, where a simplified model supporting nine to eleven overlapped pulse-amplitude modulation (PAM)-aided symbols was considered in an AWGN channel. In 1968, Saltzberg investigated the effects of FTN signaling on the achievable spectral efficiency [2]. As a result, it was shown that under the idealized simplifying assumption of a noise-less channel, binary FTN signaling relying on a rectangular shaping filter having a sinc-shaped impulse IR achieves a modest 3% higher spectral efficiency gain over Nyquist signaling without relying on equalization. Equalization techniques were developed for mitigating the FTN-specific ISI effects for improving the performance gain of FTN signaling in [58], [59]. Specifically, Lucky [58] introduced decision feedback equalization (DFE) in FTN signaling, using the term "faster-than-Nyquist" for the first time. Later, Salz [59] derived an optimal DFE based on the minimum MSE (MMSE) criterion that suffered from severe error propagation due to the high MSE of equalized FTN symbols.

2) MED ANALYSIS

In [3], Mazo investigated the MED of binary FTN signaling, in order to reveal the potential benefits achieved by FTN signaling. As a result, Mazo found that when employing the ideal sinc-shaped signaling pulses, the MED of binary FTN signaling remains unchanged in the range of $0.802 \leq \tau \leq 1$. This indicates that binary FTN signaling relying on perfect sinc-shaped signaling pulses is capable of achieving a $1/0.802 \simeq 1.25$ times higher rate than the classic Nyquist signaling scheme, at a given BER even without channel coding. Note that the maximum τ value that does not cause any MED degradation is also often referred to as the Mazo limit. Rigorous proofs of the Mazo limit were provided in [63]–[65], [67]. In 2003, Liveris and Georghiades [19] also showed the validity of the Mazo limit in FTN signaling for RRC shaping filters. Furthermore, in [68], the Mazo limit was also shown to be valid for MIMO systems.

To elaborate a little further, we show in Fig. 5 the MED of FTN signaling for the popular RRC shaping filter, where the roll-off factor was $\beta = 0$, 0.3, or 0.5, and the symbol packing ratio was varied from $\tau = 1$ to 0.02 in steps of 0.02. In the MED analysis, an exhaustive search was carried out to find the MED for a block length of $N = 16$, where BPSK modulation was assumed for the sake of simplicity. The Mazo limit decreased upon increasing the RRC roll-off factor β. More specifically, for $\beta = 0$, corresponding to the rectangular shaping filter, the MED was constant in the range of $0.8 < \tau \leq 1$ as shown by Mazo [3], while for $\beta = 0.3$ and 0.5, the MED remained unchanged in the range of $0.7 < \tau \leq 1$ and $0.64 < \tau \leq 1$, respectively. If τ falls below the Mazo limit, the MED drops.

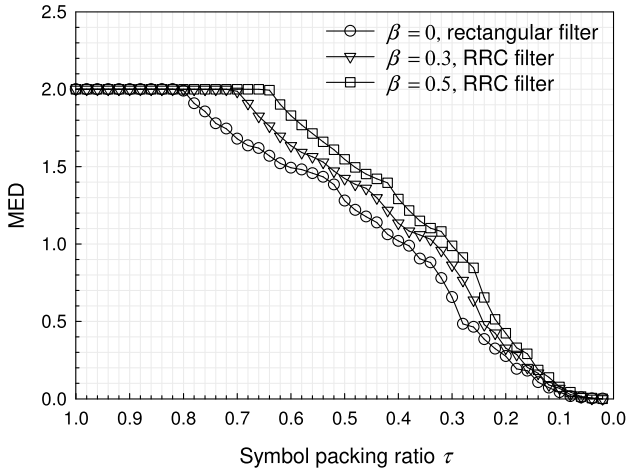

FIGURE 5. MED of FTN signaling. The roll-off factor of the RRC pulse was set to $\beta = 0$, 0.3, and 0.5. The length of the symbol sequence was set to 16, assuming BPSK.

3) OTHER TRANSCEIVER DESIGNS

Several FTN transceiver architectures were developed during the 1980s and 1990s [60]–[62]. In [60], Foschini focused his attention on an uncoded binary FTN signaling transceiver and designed a shaping filter for maximizing the MED with the aid of linear programming. However, in [60], it was reported that despite the employment of an MLSE, binary FTN signaling did not yield any significant performance advantage in comparison to Nyquist-sampled QAM. Moreover, in [61], Fihel and Sari showed that in an AWGN channel, 16-QAM-based FTN signaling was more robust against carrier-phase and timing-estimation errors than its 64-QAM-based Nyquist signaling counterpart. Furthermore, in [62], a TPC scheme was proposed for increasing the MED of FTN signaling.

C. RELATIONSHIP WITH PARTIAL-RESPONSE SIGNALING

Similar to FTN signaling, partial-response (PR) signaling increases the bandwidth efficiency by deliberately introducing controlled ISI [4], [55] which is achieved by using Gaussian signaling pulses that exhibit the smoothest possible TD evolution and hence have the narrowest possible FD representation. In other words, the objective of PR signaling is to design a smooth signaling pulse having a compact spectrum in the frequency range of $[-W, W]$, which is achieved by consciously sacrificing the orthogonality of the signaling pulses.. Thus, PR signaling achieves a higher bandwidth efficiency than classic Nyquist signaling relying on an RRC shaping filter having a bandwidth of $2W(1+\beta)$, but again, the symbol intervals of both the schemes are identical. So again, the so-called Gaussian PR signaling pulse has the most smoothly evolving PR waveform shape and hence the narrowest possible bandwidth. On the other hand, FTN signaling achieves a higher symbol rate than Nyquist signaling by reducing the symbol interval below $T_0 = 1/(2W)$ while employing the same shaping filter as Nyquist signaling, resulting in deliberate ISI.

D. NON-ORTHOGONAL FREQUENCY-DOMAIN MULTIPLEXING

Non-orthogonal symbol multiplexing has also been considered in the FD under the terminologies of non-orthogonal frequency-division multiplexing (NOFDM) and spectrally-efficient FDM (SEFDM) [69]–[86]. More specifically, NOFDM employs tighter subcarrier spacing than that defined by classic orthogonal FDM (OFDM), hence resulting in higher bandwidth efficiency. Similar to the ISI introduced by FTN signaling, inter-carrier interference (ICI) is induced between the subcarriers in NOFDM. Hence, efficient detection algorithms capable of eliminating the ICI effects have been extensively studied in the context of NOFDM [70], [72], [79], [81], [82], [84], [85]. Let us introduce the basic system model of NOFDM. The TD transmit NOFDM signal is expressed by [80], [85]

$$s(t) = \sum_{n} \sum_{k=0}^{K-1} s_n^k p(t - nT_p) e^{j2\pi k \Delta f t}, \tag{36}$$

where s_n^k is the symbol on the kth subcarrier in the nth transmit frame, while T_p is the frame duration. Moreover, $\Delta f = \alpha/T_p$ represents the subcarrier spacing of NOFDM, where α $(0 < \alpha \leq 1)$ denotes a compression factor. Note that when the signaling pulse $p(t)$ is given by a rectangular pulse and $\alpha = 1$, the transmit signal $s(t)$ corresponds to the classic OFDM signal. The system model of NOFDM when an RRC shaping filter is employed, i.e., when $p(t)$ and T_p are given by $p(t) = q(t)$ and $T_p = T_0$, respectively, is described in detail in [80], [85]. Assuming a single-frame transmission $(l = 0)$ for the sake of simplicity, the NOFDM transmit signal is represented by

$$s(t) = \sum_{k=0}^{K-1} s^k p(t) e^{j2\pi k \Delta f t}, \tag{37}$$

where s_0^k is simply denoted as s^k. The NOFDM signal received in an AWGN channel is given by

$$y(t) = s(t) + n(t). \tag{38}$$

The received signal (38) is then matched-filtered by $p^*(-t)$ and then projected onto the kth subcarrier as follows: [85]

$$y^k = \int_{-\infty}^{\infty} y(t) p^*(-t) e^{-j2\pi k \Delta f t} dt, \tag{39}$$

where y^k represents the symbol received on the kth subcarrier. The received symbol block $\mathbf{y} = [y^0, \cdots, y^{N-1}]^T \in \mathbb{C}^N$ is expressed by

$$\mathbf{y} = \mathbf{H}\mathbf{s} + \boldsymbol{\eta}, \tag{40}$$

where $\boldsymbol{\eta} = [\eta^0, \cdots, \eta^{N-1}]^T$ represents the associated noise components. The matrix $\mathbf{H} \in \mathbb{C}^{N \times N}$ in (40) is a NOFDM-specific ICI matrix whose ath row and bth column entry is given by

$$\mathbf{H}(a, b) = \int_{-\infty}^{\infty} p(t) p^*(-t) e^{j2\pi (b-a) \Delta f t} dt. \tag{41}$$

TABLE 3. Studies of MFTN signaling and their contributions.

Year	Authors	Contribution
2009	Rusek and Anderson [90]	Introduced the MFTN signaling concept and showed the Mazo limit for MFTN signaling employing an RRC shaping filter and a Gauss shaping filter. Moreover, a trellis-based detector for channel-encoded MFTN signaling was developed.
	Barbieri *et al.* [91]	Analyzed a constrained information rate of MFTN signaling employing a specified modulation scheme, showing that when using an RRC shaping filter and a Gauss shaping filter, MFTN signaling is capable of achieving higher bandwidth efficiency than its orthogonal counterpart.
2011	Dasalukunte *et al.* [93]	Proposed an MFTN receiver based on successive interference cancellation (SIC), while providing the hardware architecture of the proposed MFTN transceiver. The corresponding hardware implementation was presented in [94].
2015	Secondini *et al.* [96]	Applied MFTN signaling to a fiber optical channel and provided its experimental demonstration.
2017	Peng *et al.* [98]	Proposed MFTN signaling based on the hexagonal lattice to increase the MED, which is an extension of the hexagonal-lattice-based OFDM that is capable of reducing the effects of interference in dispersive channels [113].
	Peng *et al.* [100]	Realized PAPR reduction of MFTN signaling by extending a classic partial transmit sequence scheme developed for conventional multi-carrier modulation schemes.
2018	Liu *et al.* [101]	Investigated the PAPR distribution of MFTN signaling, showing that it depends on the symbol packing ratio, the subcarrier spacing, the number of subcarriers, and the shaping filter employed.
	Peng *et al.* [102]	Developed a clipping-based PAPR reduction scheme for MFTN signaling, while the symbol packing ratio, the subcarrier spacing, and the clipping ratio maximizing the bandwidth efficiency are numerically searched.
	Peng *et al.* [104]	Proposed an MMSE-based equalization scheme combined with SIC for MFTN signaling, which achieves the BER performance close to that achieved by the maximum *a posteriori* probability equalization scheme combined with SIC with lower computational complexity.
	Tian *et al.* [105]	Proposed a factor-graph-based receiver for MFTN signaling, where a Gaussian message-passing (GMP) algorithm was developed for the derived factor graph representation of MFTN signaling.
2020	Ma *et al.* [109]	Proposed a low-complexity GMP-based receiver for MFTN signaling in a frequency-selective fading channel, while most of the previous MFTN studies considered the AWGN channel.
	Cai *et al.* [110]	Proposed a PAPR reduction scheme for MFTN signaling based on the low-complexity selective mapping methods, which achieves the PAPR performance close to that achieved in [101] with reduced computational complexity.
	Kim and Feng [111]	Derived the capacity of MFTN signaling in a frequency-selective channel, revealing that similar to single-carrier FTN signaling, the capacity gain of MFTN signaling is due to exploiting the excess bandwidth of a shaping filter.

Moreover, the kth noise component is given by

$$\eta^k = \int_{-\infty}^{\infty} n(t)p^*(-t)e^{-j2\pi k\Delta ft}dt. \tag{42}$$

Similar to FTN signaling, the noise components $\boldsymbol{\eta}$ have a NOFDM-specific correlation as follows:

$$\mathbb{E}[\boldsymbol{\eta}\boldsymbol{\eta}^H] = N_0\mathbf{H}. \tag{43}$$

Note that in the scenario of classic OFDM, $\mathbf{H}$ is given by the identity matrix $\mathbf{I}_N$.

E. MULTI-CARRIER FTN SIGNALING

Furthermore, the concept of multi-carrier FTN (MFTN) signaling has also been studied [87]–[112], where non-orthogonal symbol packing is carried out both in the TD and FD. Note that MFTN signaling was also referred to as time-frequency packing [91], [96]. The TD transmit MFTN signal is represented by [97], [104], [105]

$$s(t) = \sum_{n=0}^{N-1}\sum_{k=0}^{K-1} s_n^k p(t - n\tau T_p)e^{j2\pi k\Delta ft}. \tag{44}$$

At the receiver, similar to NOFDM, the signal $y(t)$ received from an AWGN channel is projected onto the lth subcarrier at the mth time slot as follows: [97], [105]

$$y_m^l = \int_{-\infty}^{\infty} y(t)p^*(t - m\tau T_p)e^{-j2\pi l\Delta ft} \tag{45}$$

$$= \sum_{n=0}^{N-1}\sum_{k=0}^{K-1} s_n^k u_{n,m}^{k,l} + \eta_m^l \tag{46}$$

$$= s_m^l u_{m,m}^{l,l} + \underbrace{\sum_{n=0,n\neq m}^{N-1} s_n^l u_{n,m}^{l,l}}_{\text{The effects of ISI}} + \underbrace{\sum_{n=0}^{N-1}\sum_{k=0,k\neq l}^{K-1} s_n^k u_{n,m}^{k,l}}_{\text{The effects of ICI}} + \eta_m^l, \tag{47}$$

where we have

$$u_{n,m}^{k,l} = U_{n,m}^{k,l} e^{j2\pi(k-l)m\Delta f\tau T_p} \tag{48}$$

$$U_{n,m}^{k,l} = \int_{-\infty}^{\infty} p^*(t)p(t - (n-m)\tau T_p)e^{j2\pi(k-l)\Delta ft}dt. \tag{49}$$

The coefficient $u_{n,m}^{k,l}$ represents the effect of interference between the transmit symbols s_n^k and s_m^l [105]. Moreover, the noise component η_m^l is given by

$$\eta_m^l = \int_{-\infty}^{\infty} n(t)p^*(t - m\tau T_p)e^{j2\pi l\Delta ft}dt, \tag{50}$$

and its autocorrelation is expressed as:

$$\mathbb{E}[\eta_m^l \eta_n^{*k}] = N_0 u_{n,m}^{k,l}. \tag{51}$$

The block-based representations of the received MFTN signal in AWGN channels and in frequency-selective channels are detailed in [105] and [109], [111], respectively. The historical overview of MFTN signaling research is shown in Table 3. The concept of MFTN signaling was established in the early studies of [87]–[91]. In [87], [90], Rusek and Anderson introduced the MFTN signaling scheme and derived the two-dimensional Mazo limit for MFTN signaling employing an RRC shaping filter and a Gaussian shaping filter. In [91], Barbieri *et al.* derived the constrained information rate of

TABLE 4. Studies of TD FTN receivers and their contributions.

Year	Authors	Contribution	Channel	Channel coding
2003	Liveris and Georghiades [19]	Showed that the Mazo limit is valid for the FTN signaling scheme employing the RRC shaping filter, while proposing a channel-encoded FTN system relying on a truncated VA.	AWGN	✓
2006	Rusek and Anderson [20]	Proposed serial- and parallel-concatenated channel-coded FTN transceivers with the aid of turbo equalization.	AWGN	✓
2008	Rusek and Anderson [21]	Proposed nonbinary FTN signaling with the aid of a TPC scheme that increases the MED.	AWGN	✓
	Prlja *et al.* [22]	Developed an FTN receiver employing turbo equalization based on the BCJR algorithm.	AWGN	✓
2010	McGuire and Sima [23]	Proposed the concept of discrete-time FTN block transmission and developed sphere decoding.	AWGN	✓
2012	Prlja [24]	Developed a reduced-state BCJR algorithm for FTN signaling.	AWGN	✓
2014	Baek *et al.* [114]	Proposed the low-complexity DFE, based on QR decomposition of an FTN-induced ISI matrix.	AWGN	
2017	Bedeer *et al.* [25]	Proposed an FTN receiver based on SIC, which enables a low-complexity symbol-by-symbol detection of FTN signaling.	AWGN	
	Bedeer *et al.* [26]	Formulated detection of high-order QAM-aided FTN signaling as a non-convex optimization problem, while developing a sub-optimal demodulation scheme.	AWGN	
2018	Li *et al.* [27]	Presented a modified M-BCJR algorithm for FTN signaling to strike a flexible balance between detection performance and computational complexity.	AWGN	✓
	Fan *et al.* [115]	Introduced a channel shortening filter at the FTN receiver to reduce the complexity of MLSE.	AWGN	
	Wen *et al.* [28]	Developed a GMP-based receiver for FTN signaling over a nonlinear channel.	AWGN	✓
2019	Li *et al.* [116]	Combined FTN signaling with space-time multi-mode index modulation using GMP-based iterative detection at the receiver.	AWGN	✓
2020	Yuan *et al.* [117]	Considered FTN signaling in an uplink NOMA scenario. Both FTN-induced ISI and inter-user interference were mitigated with the aid of a message-passing algorithm.	AWGN	✓
	Li *et al.* [29]	Proposed channel-encoded FTN signaling based on channel shortening, achieving a near-capacity performance while reducing decoding complexity.	AWGN	✓

MFTN signaling employing a realistic discrete modulation scheme, showing that when using an RRC shaping filter and a Gaussian shaping filter, MFTN signaling achieves a higher bandwidth efficiency than its orthogonal counterpart. An efficient detection scheme for MFTN signaling has been developed in [90], [91], [93], [97], [104], [105], [109], which considers both the effects of ISI and ICI. Moreover, the peak-to-average power ratio (PAPR) problem of MFTN signaling caused by multi-carrier transmission has been considered in [100]–[102], [108], [110]. Furthermore, in [111], Kim and Feng derived the capacity of MFTN signaling in a frequency-selective channel for the first time, revealing that similar to single-carrier FTN signaling [5], the capacity gain of MFTN signaling is due to exploiting the excess bandwidth of the shaping filter employed.

IV. TIME-DOMAIN FTN RECEIVERS

In this section, we review the family of TD FTN equalizers.

A. TRELLIS-BASED FTN RECEIVERS

In [19], Liveris and Georghiades developed an efficient iterative decoding algorithm for turbo-encoded FTN signaling, as an evolution from the uncoded FTN signaling scheme reviewed in Section III-B. It was shown in [19] that turbo-encoded FTN signaling relying on the parameters $(\tau, \beta) = (0.9, 0.1)$ achieved a BER performance similar to that of its conventional Nyquist signaling counterpart.

After [19], a range of efficient TD FTN receivers were reported, as listed in Table 4. In [20], Rusek and Anderson developed a parallel-concatenated channel-encoded FTN system relying on a unity-rate recursive convolutional code and an iterative turbo equalizer, achieving better performance than the channel-encoded FTN system of [19]. As a further development, Rusek and Anderson [21] proposed an efficient algorithm for determining the MED of nonbinary PAM-aided FTN signals. This was used for designing a TPC for improving the BER performance, where a trellis-based decoder employing the M-algorithm was harnessed at the receiver. In [22], Prlja *et al.* proposed an improved channel-encoded FTN signaling architecture based on the Bahl, Cocke, Jelinek, and Raviv (BCJR) decoding algorithm, and evaluated its convergence behavior with the aid of extrinsic information transfer (EXIT) charts. It was also demonstrated that upon increasing the roll-off factor β of an RRC shaping filter, the achievable BER performance improved, as a benefit of the rapidly decaying RRC signaling pulse.

Although the aforementioned FTN receivers are capable of successfully demodulating FTN symbols even in low-τ scenario, the computational complexity of the trellis-based TD receivers exponentially increases upon increasing both the effective tap length and the constellation size employed. In response, reduced-state trellis-based FTN receivers were developed in [24], [118], [119]. In [24], a novel M-algorithm based BCJR (M-BCJR) decoding algorithm was conceived for channel-encoded FTN signaling, where M dominant paths were retained at each trellis stage. Furthermore, in [27], the M-BCJR algorithm was further developed for striking a

TABLE 5. Studies of frequency-domain receivers for FTN signaling and their contributions.

Year	Authors	Contribution	Channel	Channel coding
2013	Sugiura [30]	Proposed the MMSE-based FDE of uncoded FTN signaling, which enables low-complexity detection of FTN signals.	Frequency-selective	
2015	Sugiura and Hanzo [31]	Extended the hard-decision FDE of [30] to its SoD counterpart.	Frequency-selective	✓
	Fukumoto and Hayashi [121]	Proposed the hard-decision noise-whitening MMSE-based FDE that takes into account the effects of an FTN-specific noise correlation.	AWGN	
	Dinis *et al.* [32]	Incorporated the FTN signaling concept into the HARQ-based transceiver.	Doubly selective	
2016	Yuan *et al.* [33]	Considered the MMSE-FDE-aided FTN receiver for a doubly selective fading channel.	Doubly selective	✓
	Wu *et al.* [34]	Proposed an FD iterative message-passing algorithm for FTN signaling.	AWGN	✓
2017	Ishihara and Sugiura [35]	Proposed an FDE-aided iterative joint CE and DD for FTN signaling.	Frequency-selective	✓
	Ishihara and Sugiura [36]	Proposed an FDE-aided FTN signaling combined with the SCIM concept.	Frequency-selective	
	Nakao *et al.* [37]	Proposed a dual-mode SCIM concept, which was combined with FTN signaling in order to enhance the achievable spectral efficiency.	Frequency-selective	
2018	Ishihara and Sugiura [38]	Proposed the FDE-aided DFTN signaling concept that dispenses with any CE in a frequency-flat fading channel.	Frequency-flat	
	Shi *et al.* [39]	Proposed an FD CE and DD scheme based on a message-passing algorithm for a factor graph.	Frequency-selective	✓
2019	Sagayama *et al.* [40]	Extended the DFTN scheme [38] to support 16-point star-QAM.	Frequency-flat	

flexible tradeoff between the detection performance attained and the computational complexity imposed.

While the main focus of the studies in [24], [27] was to reduce the complexity of the trellis search, in [115] MMSE-based channel shortening was conceived for reducing the effective ISI contamination duration of FTN signaling, hence mitigating the complexity of the Viterbi algorithm without degrading the achievable BER performance. More recently, in [29], the channel shortening scheme of [115], which was originally developed for uncoded FTN signaling, was further developed by including channel-coding.

B. FURTHER STUDIES OF TIME-DOMAIN FTN RECEIVERS

In addition to the above-mentioned trellis-based receivers, other TD detection algorithms have also been developed for FTN signaling. Explicitly, in [23], McGuire and Sima constructed a sphere decoding algorithm for efficiently detecting FTN symbols. In [114], a DFE based on QR decomposition of the FTN-induced ISI matrix was proposed. Moreover, in [25], [120], SIC was employed for reducing the detection complexity of FTN signaling. In [28], an FTN receiver relying on a GMP algorithm based on a factor graph was proposed, where the FTN-specific correlated noise was approximated by an autoregressive process with the objective of reducing the detection complexity. A similar message-passing algorithm relying on a factor graph was developed for FTN signaling, which was combined with space-time multi-mode index modulation in [116] and also with non-orthogonal multiple-access (NOMA) in [117].

V. FREQUENCY-DOMAIN FTN RECEIVERS

In this section, we review the studies of FD FTN receivers. As discussed in Section IV, the TD trellis-based FTN receivers are eminently suitable for demodulating FTN signaling. However, the above-mentioned trellis-based receivers were typically used in the context of AWGN channels, while frequency-selective fading dispersive channels were not considered, since the computational complexity may become excessive owing to the additional ISI. As a remedy, an FD FTN receiver facilitates low-complexity detection of FTN signals even in low-τ and high-dispersion channels. Hence, in this section, we review pertinent studies of FD FTN receivers. The related literature is summarized in Table 5.

A. HARD-DECISION FDE-AIDED FTN DEMODULATOR

The FD FTN receiver concept was originally proposed by Sugiura [30]. Historically, the low-complexity frequency-domain equalization (FDE) philosophy was originally developed for single-carrier frequency-division multiple access (SC-FDMA) of Nyquist signaling [122], [123], which was then further developed by Sugiura [30] for his MMSE-based FDE of FTN signaling. In Sugiura's proposal, the first 2ν symbols of $\mathbf{s}$ are copied to the end of $\mathbf{s}$ as cyclic prefix (CP) at the transmitter. Hence, the $(N+2\nu)$-length symbol vector $[s_0, \cdots, s_{N-1}, s_0, \cdots, s_{2\nu-1}]^T$ is transmitted using the FTN-specific symbol interval $T = \tau T_0$. At the receiver, the first and last ν symbols are discarded from the $(N+2\nu)$-length received sample stream, yielding the received samples of

$$\begin{aligned}\mathbf{y} &= [y_0, y_1, \cdots, y_{N-1}]^T \in \mathbb{C}^N \\ &= \mathbf{G}_c\mathbf{s} + \boldsymbol{\eta}. \end{aligned} \tag{52}$$

$\mathbf{G}_c$ in (52) is a circulant matrix whose first column is given by $[g(-\nu T), \cdots, g(0), \cdots, g(\nu T), 0, \cdots, 0]^T \in \mathbb{C}^N$ [30]. The eigenvalue decomposition of $\mathbf{G}_c$ is given

by [30], [122], [123]

$$\mathbf{G}_c = \mathbf{Q}\Lambda_c\mathbf{Q}^H, \tag{53}$$

where the matrix $\mathbf{Q}$ is the normalized discrete Fourier transform (DFT) matrix, whose mth-row and nth-column element is represented by $1/\sqrt{N}\exp(-2\pi j(n-1)(m-1)/N)$. Moreover, Λ_c is the diagonal eigenvalue matrix, whose diagonal elements are calculated by the non-normalized DFT of the first column of $\mathbf{G}_c$. Hence, the TD FTN symbols are estimated as follows:

$$\hat{\mathbf{s}} = \mathbf{Q}\mathbf{W}\mathbf{Q}^H\mathbf{y}, \tag{54}$$

where $\mathbf{W}$ is an MMSE-based FDE weight matrix, given by the diagonal matrix

$$\mathbf{W}_{\text{white}} = \Lambda_c^H\left(\Lambda_c\Lambda_c^H + \frac{N_0}{\sigma_s^2}\mathbf{I}_N\right)^{-1}. \tag{55}$$

This representation indicates that the complexity order of the MMSE-based FDE is as low as $N\log N$, since the multiplications of the DFT and inverse DFT (IDFT) matrices in (54) are efficiently implemented by the fast Fourier transform (FFT). On the other hand, as mentioned above, the complexity order of the TD trellis-based equalization typically increases exponentially both with the block size and with the CIR length.

The weight matrix (55) proposed by Sugiura in [30] was derived while ignoring the effects of the FTN-specific noise correlation. To improve the achievable detection performance, in [121], a weight matrix taking into account the effects of noise correlation was formulated as

$$\mathbf{W}_{\text{ideal}} = \Lambda_c^H\left(\Lambda_c\Lambda_c^H + \frac{1}{\sigma_s^2}\mathbf{Q}^H\mathbb{E}\left[\boldsymbol{\eta}\boldsymbol{\eta}^H\right]\mathbf{Q}\right)^{-1}. \tag{56}$$

However, since the FTN-specific noise correlation matrix $\mathbb{E}\left[\boldsymbol{\eta}\boldsymbol{\eta}^H\right]$ is not diagonal, the ideal MMSE weights (56) no longer constitute a diagonal matrix. Hence, in order to maintain the diagonal weight matrix structure of MMSE-based FDE [122], [123], the ideal MMSE weights (56) were approximated by a diagonal matrix as follows:

$$\mathbf{W}_{\text{color}} = \Lambda_c^H\left(\Lambda_c\Lambda_c^H + \frac{N_0}{\sigma_s^2}\Phi\right)^{-1}, \tag{57}$$

where we have

$$\Phi = \text{diag}\left\{\Phi[0], \Phi[1], \cdots, \Phi[N-1]\right\} \tag{58}$$

$$\Phi[n] = \frac{1}{N}\sum_{l=0}^{N-1}\sum_{m=0}^{N-1} g((l-m)T)\exp\left(\frac{2\pi j(l-m)n}{N}\right). \tag{59}$$

Here, $N_0\Phi_\eta[n]$ is the nth diagonal element of $\mathbb{E}[\boldsymbol{\eta}\boldsymbol{\eta}^H]$. The noise-whitening diagonal MMSE matrix (57) facilitates low-complexity symbol-by-symbol detection, yet achieving better BER performance than the original FDE matrix of (55). The MMSE-based FDE algorithm is also readily applied to frequency-selective fading channels [30], [31], [35] by appropriately extending the CP length. As an explicit benefit of the low-complexity MMSE-based FDE, the resultant FTN receiver is also suitable for highly dispersive fading channels.

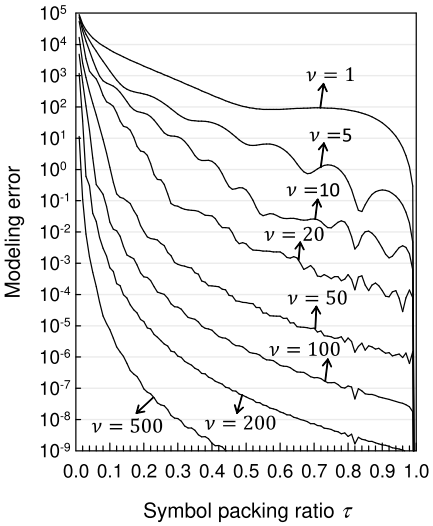

FIGURE 6. Modeling error due to the approximated circulant matrix [30]. Here, the block length and the CP length were set to $N = 1024$ and $\nu = 1$, 5, 10, 20, 50, 100, 200, and 500, respectively. The symbol packing ratio was varied from $\tau = 1$ to 0.01 in steps of 0.01. The roll-off factor was set to $\beta = 0.22$.

Note that in the above-mentioned CP-assisted FTN system, the duration of the FTN-induced ISI, which is theoretically infinite, is truncated to the finite length ν, in order to approximate the circulant matrix of (52). Fig. 6 shows the effects of the modeling error imposed by the approximated circulant matrix $\mathbf{G}_c$ [30]. The block length was set to $N = 1024$ and CP lengths of $\nu = 1$ 5, 10, 20, 50, 100, 200, and 500 were considered. The symbol packing ratio was varied from $\tau = 1$ to 0.01 in steps of 0.01, while the roll-off factor was maintained at $\beta = 0.22$. Observe in Fig. 6 that the modeling error decreased upon increasing the CP length. For example, upon increasing the CP length from $\nu = 5$ to $\nu = 100$, the square error at $\tau = 0.5$ was decreased from 6.47 to 5.02×10^{-7}. The CP length has to be sufficiently long so that the associated modeling error becomes sufficiently low [30].

Fig. 7 shows the achievable BER performance of the uncoded FTN signaling scheme employing the MMSE weights of $\mathbf{W}_{\text{color}}$ in (57) and $\mathbf{W}_{\text{white}}$ in (55), where the roll-off factor, the block length and the CP length were set to $\beta = 0.22$, $N = 1024$ and $2\nu = 20$, respectively. The symbol packing ratio was set to $\tau = 1, 0.9, 0.8, 0.7$, as well as 0.6, and BPSK modulation was assumed. Note that the power penalty imposed by the CP was ignored. As shown in Fig. 7, the FTN signaling scheme employing the noise-whitening MMSE weights of $\mathbf{W}_{\text{color}}$ in (57) achieved better BER performance than that employing the MMSE weights of $\mathbf{W}_{\text{white}}$ in (55). The performance advantage of the noise-whitening MMSE-based FDE algorithm increased upon reducing the symbol packing ratio τ.

Moreover, Fig. 8 shows the achievable BER performance of FTN signaling employing the approximated noise-whitening MMSE weights $\mathbf{W}_{\text{color}}$ of (57) and the ideal MMSE weights $\mathbf{W}_{\text{ideal}}$ of (56). The symbol packing ratio was set to $\tau = 0.9$, 0.83, 0.8, and 0.7, while the roll-off factor

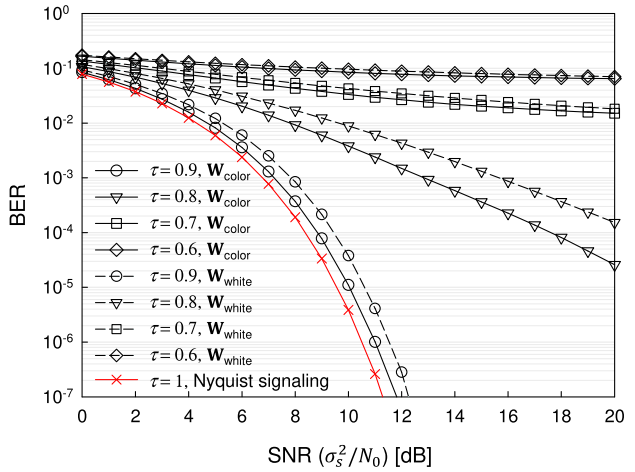

FIGURE 7. Achievable BER performance of the uncoded FTN signaling scheme using the FDE weights $\mathbf{W}_{\text{white}}$ and $\mathbf{W}_{\text{color}}$. We employed a roll-off factor of $\beta = 0.22$, block length of $N = 1024$, and CP length of $2\nu = 20$. The symbol packing ratio was varied from $\tau = 1$ to 0.6 in steps of 0.1. Moreover, the BPSK modulation scheme was used.

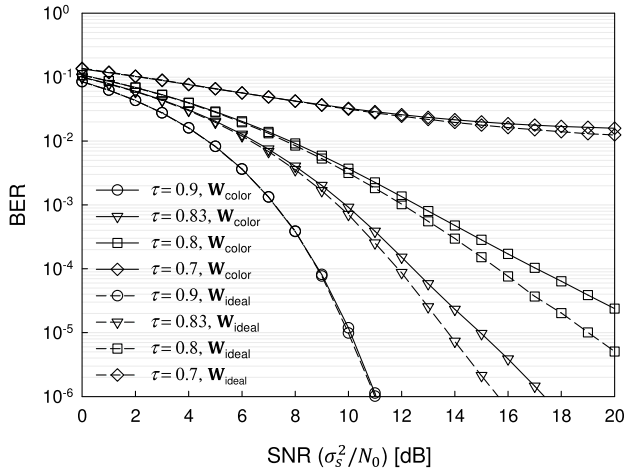

FIGURE 8. Achievable BER performance of the uncoded FTN signaling scheme using noise-whitening FDE weight $\mathbf{W}_{\text{color}}$ and ideal FDE weight $\mathbf{W}_{\text{ideal}}$. The roll-off factor β was set to $\beta = 0.22$, while the symbol's packing ratio τ was set to $\tau = 0.9, 0.83, 0.8,$ and 0.7.

was set to $\beta = 0.22$. A block length of $N = 128$ and CP length of $2\nu = 20$ were used. As shown in Fig. 8, it was found that in the low-rate scenario of $\tau = 0.9$, the BER of the noise-whitening FDE-aided FTN signaling system was comparable to that of its ideal FDE-aided counterpart. However, in the range of $\tau < 0.9$, the performance degradation due to the approximation of noise correlation is visible.

B. SoD FDE-AIDED ITERATIVE FTN RECEIVERS

In general, powerful channel coding and iterative decoding have to be employed in order to achieve a high throughput gain with the aid of FTN signaling [4], [31]. In [31], the hard-decision MMSE-based FDE of [30] was extended to its soft-decision (SoD) FDE counterpart resulting in a multi-stage serially concatenated turbo-coded FTN system. As a result, near-capacity detection performance was

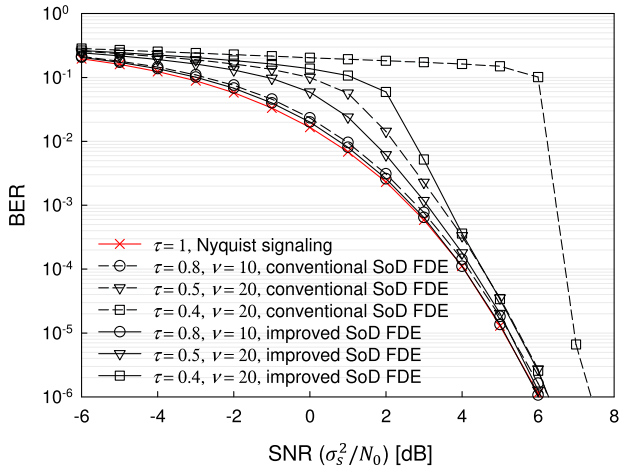

FIGURE 9. Achievable BER performance of the two-stage RSC-encoded FTN signaling system, employing the SoD FDE of [35] and the SoD FDE in an AWGN channel. The roll-off factor was set to $\beta = 0.22$, while the symbol packing ratio was set to $\tau = 0.8, 0.5,$ and 0.4. The CP length was set to $\nu = 10$ for $\tau = 0.8$ and $\nu = 20$ for $\tau = 0.5, 0.4$.

achieved while maintaining low detection complexity. Note that the SoD FDE of [31] did not take into account the effects of FTN-specific noise correlation. In [35], an improved SoD-FDE algorithm was proposed using an extension of the hard-decision-based noise-whitening MMSE weights (55).

Fig. 9 shows the BER performance of the two-stage turbo-coded FTN signaling system employing the SoD FDE of [31], [35] in an AWGN channel using BPSK modulation. We considered the same turbo-coded architecture as that of [31], [35], where the half-rate recursive systematic coding (RSC)(2, 1, 2) code having octal generator polynomials of (3, 2) was employed, while the interleaver length and the number of iterations were set to $2^{18} = 262,144$ and 21, respectively. For the sake of simplicity, the effects of interblock interference (IBI) were not taken into account. More specifically, 2^{18} channel-encoded bits were divided into multiple blocks having N bits. Then, multiple blocks were independently modulated and transmitted [15], [31], [35]. We employed the FTN signaling parameters of $(\tau, \beta, \nu) = (0.8, 0.22, 10), (0.5, 0.22, 20),$ and $(0.4, 0.22, 20)$. Moreover, we also characterized the ISI-free Nyquist bound. As shown in Fig. 9, the pair of SoD-FDE receivers achieved a low BER, even in the high-rate scenario of $\tau = 0.4$. Furthermore, for $\tau = 0.4$, the noise-whitening SoD-FDE receiver of [35] achieved a BER close to the Nyquist-criterion-based achievable bound. Additionally, note that in [31], the achievable BER performance of the three-stage-concatenated turbo-coded FTN signaling system relying on the SoD FDE was also investigated in both AWGN and frequency-selective Rayleigh fading channels.

While the MMSE-based FDE-aided FTN signaling allows us to carry out low-complexity detection, the achievable performance may be exceeded by its TD counterpart, which has a higher complexity. In [124], FDE and the TD BCJR algorithm were compared in the context of a half-rate channel-encoded FTN signaling scheme, and the BCJR algorithm was shown

to achieve better BER performance than the FDE at the cost of increased detection complexity. However, a relatively low code length of $N = 2004$ was considered in [124]; hence, the performance gap may be reduced in a scenario using a higher code length.

C. FURTHER STUDIES RELATED TO FREQUENCY-DOMAIN FTN RECEIVERS

In [32], hybrid automatic repeat request (HARQ) was used in conjunction with the FDE-aided FTN signaling scheme in the doubly selective fading channel. Similarly, in [33], FDE was employed by an FTN signaling scheme experiencing a doubly selective fading channel. In [32], [33], it was shown that FTN signaling has the potential to achieve a higher throughput than Nyquist signaling in a doubly selective channel. Moreover, in [36], FDE was employed by the FTN signaling scheme combined with single-carrier index modulation (SCIM) [125], which is sometimes referred to as FTN-index modulation (FTN-IM) signaling. In [36], [126], FTN-IM signaling achieved a better BER and information rate than the conventional FTN signaling in a low-rate scenario. Moreover, in [37], the concept of dual-mode IM was combined with FTN-IM signaling, in order to improve the bandwidth efficiency. Furthermore, FD CE was developed for FTN signaling in [35], [39]. In [38], [40], FDE-aided differential FTN (DFTN) signaling and noncoherent detection were proposed for dispensing with pilot-assisted CE.

VI. CHANNEL ESTIMATION ISSUES FOR FTN SIGNALING

A. CHANNEL ESTIMATION FOR FTN SIGNALING

In most studies of FTN signaling, it was typically assumed that the channel state information (CSI) is perfectly known at the receiver for the sake of simplicity. In [41], the conventional Nyquist-sampling-based orthogonal pilot symbols were added in front of the FTN signaling data block, where a time-limited Gaussian shaping filter was employed for suppressing the FTN-induced ISI. Exploiting the conventional Nyquist-sampling-based orthogonal pilot symbols is a straightforward solution for CE. However, when employing a bandlimited shaping filter, a sufficiently long guard interval is required between the pilot block and FTN data symbols.

To achieve accurate CE, while reducing the pilot overhead, FTN-based pilot (FTNP) sequence was exploited in [35], [39], [42]. In [42], Wu *et al.* proposed a joint CE and data detection (DD) scheme exploiting an FTNP sequence for the first time, where a Gaussian message-passing algorithm was employed. The FTNP-aided CE scheme of [42] achieved good CE performance. However, the associated complexity grew with the cube of the effective ISI tap length [39].

In contrast to the TD iterative joint CE and DD scheme of [42], a low-complexity FD counterpart was developed in [35], [39]. In [35], Ishihara and Sugiura proposed FTNP-aided CE based on low-complexity MMSE-based FDE [30], [31]. The FDE-aided joint iterative CE and DD scheme was conceived for both uncoded and channel-encoded FTN signaling, where the demodulated FTN data symbols were exploited as a long FTNP sequence. As a benefit of the iterative CE and DD process, a detection performance close to the idealized BER bound assuming perfect CSI was achievable, while minimizing the FTNP length.

Furthermore, in [39], Shi *et al.* presented an FD message-passing-aided CE scheme, motivated by its TD counterpart of [42]. In [39], FD joint CE and DD without relying on CP was proposed, where the effects of inter-block interference (IBI) were taken into account. Moreover, in order to reduce the CE and DD complexity, the effects of the FTN-specific noise correlation characterized by (32) were approximately modeled in a circulant channel matrix. In [39], it was shown that the approximation error increases upon reducing the τ value. While a quasi-static frequency-selective fading channel was assumed in [35], [42], a time-varying scenario was considered in [39]. In [39], it was demonstrated that for $\tau = 0.6$ and $\beta = 0.5$, LDPC-coded FTN signaling using quadrature phase-shift keying (QPSK) achieved a good BER close to that of its Nyquist-based counterpart in a time-varying dispersive channel.

Furthermore, in [43], FTN signaling was employed in the NOMA uplink based on a random access protocol, where both CE and DD, as well as user-activity tracking were iteratively carried out with the aid of the expectation maximization (EM)-based message-passing algorithm at a base station. Moreover, in [127], [128], FTNP sequence was designed for minimizing the associated FD CE error.

B. DIFFERENTIAL FTN SIGNALING AND NONCOHERENT DETECTION

Although several CE schemes have been developed, as reviewed in Section VI-A, typically an iterative CE and DD procedure is required at the receiver in order to obtain sufficiently accurate CSI [35], [39], [42], [43]. Moreover, imposing a pilot overhead is unavoidable, even if FTNP sequence is used. To circumvent this limitation, a DFTN signaling concept was proposed in [38], where differential encoding and noncoherent detection allow us to dispense with CE at the receiver, hence achieving a pilot-free low-complexity transceiver. More specifically, the FTN-induced ISI was mitigated at the receiver with the aid of FDE based on the FTN parameters, i.e., τ and β, known in advance of transmission. Then, noncoherent detection was carried out for the equalized DFTN symbols. It was shown by the simulation results of [38] that DFTN signaling and noncoherent detection can operate reliably in a frequency-flat fading channel while suffering from a noise-doubling effect, similar to that of conventional Nyquist-sampling-based differential modulation. Moreover, in a rapidly time-varying fading channel, the noncoherent DFTN scheme has the potential of achieving better BER performance than its conventional coherent FTN counterpart due to the out-of-dated estimated channels. This is particularly so in high-Doppler scenarios, because every time the vehicular speed is doubled, the pilot overhead also must be doubled, hence wasting a lot of pilot-power.

TABLE 6. Studies of channel estimation for FTN signaling and noncoherent DFTN signaling.

Year	Authors	Contribution
2014	Hirano *et al.* [41]	Exploited Nyquist-based orthogonal pilot to estimate the channel of FTN data symbols, where a time-limited Gaussian shaping filter was used to mitigate the FTN-induced ISI effects.
2017	Wu *et al.* [42]	Conceived TD message-passing-aided CE for FTN signaling, where an FTNP sequence was exploited to improve bandwidth efficiency.
	Ishihara and Sugiura [35]	Proposed FD iterative CE and DD for FTN signaling, where low-complexity MMSE-based FDE [30, 121] was used to support CE by an FTNP sequence.
2018	Ishihara and Sugiura [38]	Proposed DFTN signaling to dispense with CE at the receiver in a frequency-flat fading channel. Noncoherent detection was carried out after MMSE-based FDE of FTN signaling.
	Shi *et al.* [39]	Extended the TD iterative joint CE and DD scheme of [42] to an FD counterpart for a time-varying frequency-selective fading channel.
2019	Sagayama *et al.* [40]	Developed 16-point star-QAM-aided FTN signaling, where the constellation was optimized to minimize the average BER.
2020	Yuan *et al.* [43]	Proposed the EM-based message-passing algorithm for carrying out iterative CE and DD as well as user activity tracking in the uplink FTN-NOMA scenario.

While in the DFTN scheme of [38], PSK was considered, in [40], 16-point star QAM was employed, where the ring ratio of the star-QAM constellation was optimized to maximize the theoretical BER value at each SNR. It was shown in [40] that the DFTN signaling scheme using 16-point star-QAM achieved better BER than that of the 16-point PSK constellation proposed in [38].

VII. PRECODED FTN SIGNALING

Precoding schemes have also been developed for FTN signaling schemes for several reasons. In this section, we review the family of precoded FTN signaling schemes, which are summarized in Table 7. Precoded FTN signaling was initially proposed for increasing the MED of FTN signaling [21], [60], [62].

A. SYSTEM MODEL OF LINEAR PRECODING

To overcome the FTN-induced ISI effects, linear precoding based on matrix factorization was conceived in [13]–[15], [44], [45], [49], [134]. Here, we assume that the FTN-induced ISI matrix $\mathbf{G}$ of (31) is diagonalized in order to eliminate the ISI effects at the receiver. In general, the linearly precoded symbol block is represented by [15]

$$\begin{aligned}\mathbf{x} &= [x_0, \ \cdots, \ x_{N-1}]^T \in \mathbb{C}^N \\ &= \mathbf{Fs}, \end{aligned} \tag{60}$$

where $\mathbf{F} \in \mathbb{C}^{N\times N}$ is a linear TPC matrix. The corresponding transmit signal after passing through a shaping filter $q(t)$ is given by

$$x(t) = \sum_{n=0}^{N-1} x_n q(t - nT). \tag{61}$$

Similar to (24), the average transmit energy of the N-length precoded FTN signals $x(t)$ is calculated by [13], [15]

$$E_p = \mathbb{E}\left[\sum_{l=0}^{N-1}\sum_{m=0}^{N-1} x_l x_m^* g((l-m)T)\right] \tag{62}$$

$$= \mathbb{E}[\mathbf{x}^H\mathbf{Gx}] \tag{63}$$

$$= \mathbb{E}[\mathbf{s}^H\mathbf{F}^H\mathbf{GFs}]. \tag{64}$$

In order to maintain the average power, the relationship of $E_p = E_N$ has to be satisfied.

Under the assumption of an AWGN channel, the matched-filtered received signal is given by

$$r(t) = \sum_{n=0}^{N-1} x_n g(t - nT) + \eta(t). \tag{65}$$

Then, the sampled signal block is represented by

$$\mathbf{r} = [r_0, \cdots, r_{N-1}]^T \in \mathbb{C}^N \tag{66}$$

$$= \mathbf{Gx} + \boldsymbol{\eta} \tag{67}$$

$$= \mathbf{GFs} + \boldsymbol{\eta}, \tag{68}$$

where $r_k = r(kT)$ is the kth sampled signal. For the sake of simplicity, we only consider a single block transmission in the rest of this paper. Hence, the detrimental effects of IBI are ignored.

Furthermore, the received sample block $\mathbf{r}$ of (68) may be multiplied by the weights $\mathbf{W} \in \mathbb{C}^{N\times N}$ as follows:

$$\mathbf{r}_d = \mathbf{Wr} \tag{69}$$

$$= \mathbf{WGFs} + \mathbf{W}\boldsymbol{\eta} \in \mathbb{C}^N. \tag{70}$$

B. EIGENDECOMPOSITION-BASED PRECODED FTN SIGNALING

In [44], [45], precoded FTN signaling based on eigenvalue decomposition (EVD) was proposed.[1] To elaborate a little further, in [44], [45], the FTN-induced ISI matrix $\mathbf{G}$ was factorized based on the singular value decomposition (SVD). Note that since the matrix $\mathbf{G}$ is real-valued and symmetric, the SVD of $\mathbf{G}$ is equivalent to the EVD [44]. Hence, the SVD-precoded FTN signaling scheme proposed in [44], [45] is also referred to as EVD-precoded FTN signaling in this paper. The FTN-induced ISI matrix $\mathbf{G}$ is decomposed with the aid of the EVD as follows:

$$\mathbf{G} = \mathbf{V}\Lambda\mathbf{V}^T, \tag{71}$$

where $\mathbf{V} \in \mathbb{R}^{N\times N}$ is a unitary matrix, and $\Lambda \in \mathbb{R}^{N\times N}$ is a diagonal matrix consisting of the eigenvalues of

[1] EVD-based TPC was also developed for NOFDM in [71], [85].

TABLE 7. Studies of precoded FTN signaling and their contributions.

Year	Authors	Contribution
1995	Wang and Lee [62]	Proposed a precoding scheme to maximize the MED of two different FTN signaling codes.
2008	Rusek and Anderson [21]	Proposed a nonbinary FTN signaling relying on a precoding scheme that increases the MED.
2010	Kim and Bajcsy [129]	Investigated the possibility of spectrum broadening imposed on precoded FTN signaling, where the bandwidth of precoded FTN signaling is not broadened if and only if a shaping filter is strictly bandlimited.
2015	Gattami *et al.* [13]	Conceived a precoding scheme based on an ISR of the ISI matrix. It was also proved that ISI matrix $\mathbf{G}$ is positive definite, and hence its unique square root $\mathbf{G}^{\frac{1}{2}}$ exists.
2016	Kim [14]	Revealed several properties of the FTN-induced ISI matrix, including its positive definiteness and eigenvalue distribution. The capacity of FTN signaling was derived based on EVD of the FTN-induced ISI matrix.
2017	Jana *et al.* [47]	Introduced THP in FTN signaling and extended it to the LPE-aided counterpart.
	Qian *et al.* [45]	Conceived a bit-loading scheme for EVD-precoded FTN signaling to increase the MED.
2018	Spano *et al.* [46]	Proposed a precoding scheme that equalizes ISI imposed by FTN signaling and multi-user transmission over a MISO channel.
	Jana *et al.* [130]	Extended the LPE-aided FTN signaling of [47] to dual-polarized FTN signaling.
2019	Che *et al.* [131]	Proposed TD linear filtering to increase a constrained information rate of the FTN signaling with L-point QAM schemes, where the tap coefficients were optimized with the aid of particle swarm optimization.
	Wen *et al.* [132]	Designed a TD MMSE filter that minimizes the MSE between the transmitted symbols and the received symbols after equalization.
	Ishihara and Sugiura [15]	Proposed EVD-precoded FTN signaling combined with optimal and truncated power allocation, which was capable of attaining a higher information rate than the conventional FTN signaling.
2020	Wang *et al.* [48]	Proposed a SIC-based nonlinear receiver to mitigate residual ISI of THP-aided FTN signaling.
2021	An *et al.* [133]	Carried out an experiment employing THP-FTN signaling using 16-point QAM in a single-mode fiber optical communication channel, showing 21.73% rate enhancement.
	Li *et al.* [49]	Introduced Cholesky-decomposition-based TPC into FTN signaling, which has the equivalent system model and the same BER performance as those of EVD-precoded FTN signaling in conjunction with power allocation [15].
	Sugiura [50]	Investigated the analytical information and secrecy rates of the EVD-precoded FTN signaling in quasi-static frequency-flat fading.
	Ishihara and Sugiura [18]	Proposed EVD-precoded FTN signaling combined with optimal power allocation for the scenario of a frequency-selective fading channel.
	Chaki *et al.* [51]	Amalgamated the SCIM concept with EVD-precoded FTN signaling combined with optimal power allocation, showing that the proposed FTN-IM scheme achieved the ISI-free BER bound in the AWGN channel for $\tau \geq 1/(1+\beta)$.

$[\lambda_0, \lambda_1, \cdots, \lambda_{N-1}]$ represented in descending order. Note that since the ISI matrix $\mathbf{G}$ deterministically depends on both τ and β, its EVD is calculated offline in advance of transmissions [15], [45]. As proved in [13], [14], for a finite block length N, $\mathbf{G}$ is positive definite, hence there are N non-zero eigenvalues.

By letting the TPC matrix $\mathbf{F}$ and the weight matrix $\mathbf{W}$ be $\mathbf{F} = \mathbf{V}$ and $\mathbf{W} = \mathbf{V}^T$, respectively, the received signals of (70) are reformulated as:

$$\begin{aligned} \mathbf{r}_d &= \mathbf{V}^T\mathbf{r} \in \mathbb{C}^N && (72)\\ &= \mathbf{V}^T\mathbf{G}\mathbf{V}\mathbf{s} + \mathbf{V}^T\boldsymbol{\eta} && (73)\\ &= \Lambda\mathbf{s} + \boldsymbol{\eta}_v, && (74) \end{aligned}$$

where $\boldsymbol{\eta}_{\mathrm{v}} = \mathbf{V}^T\boldsymbol{\eta}$. As seen in (74), the ISI matrix $\mathbf{G}$ is diagonalized, and thus the received signals $\mathbf{r}_d$ are regarded as N independent parallel streams. Moreover, the covariance matrix of $\boldsymbol{\eta}_v$ is formulated as [15], [44]

$$\begin{aligned} \mathbb{E}[\boldsymbol{\eta}_v\boldsymbol{\eta}_v^H] &= \mathbf{V}^T\mathbb{E}[\boldsymbol{\eta}\boldsymbol{\eta}^H]\mathbf{V} && (75)\\ &= N_0\mathbf{V}^T\mathbf{G}\mathbf{V} && (76)\\ &= N_0\Lambda. && (77) \end{aligned}$$

Hence, the associated noise components are whitened by the weight matrix $\mathbf{W} = \mathbf{V}^T$, and the noise variance in the kth stream is represented by $N_0\lambda_k$. With the aid of precoding at the transmitter and weighting at the receiver, the EVD-precoded FTN signals are demodulated in a low-complexity symbol-by-symbol manner [15], [44], [45].

Furthermore, according to (64), the average transmit energy per N-length block is calculated by

$$\begin{aligned} E_p &= \mathbb{E}[\mathbf{s}^H\mathbf{V}^T\mathbf{G}\mathbf{V}\mathbf{s}] && (78)\\ &= \mathbb{E}[\mathbf{s}^H\Lambda\mathbf{s}] && (79)\\ &= \sum_{k=0}^{N-1}\lambda_k\cdot\mathbb{E}[|s_k|^2] && (80)\\ &= N\sigma_s^2, && (81) \end{aligned}$$

where we have $\mathbb{E}[|s_k|^2] = \sigma_s^2$ and $\sum_{k=0}^{N-1}\lambda_k = \mathrm{trace}\{\mathbf{G}\} = N$ [15]. Hence, it is confirmed that EVD-based precoding does not change the average transmit energy.

As seen from (74) and (77), the SNR of the kth stream is given by $\lambda_k\sigma_s^2/N_0$. Depending on the τ and β values, the ISI matrix $\mathbf{G}$ may include quite low eigenvalues [14], [15], [45], which makes it difficult to detect the associated symbols. It was shown in [14] that the kth eigenvalue of $\mathbf{G}$ is approximated by

$$\lambda_k \simeq \frac{1}{\tau}H_{\mathrm{fo}}(f_k) \quad \text{for} \quad f_k = \frac{k}{N\tau T_0}, \tag{82}$$

where $H_{fo}(f)$ in (87) is the folded pulse spectrum of a shaping filter having the frequency response of $H(f)$, which is defined by [5]

$$H_{\mathrm{fo}}(f) \triangleq \sum_{k=-\infty}^{\infty}\left|H\left(f+\frac{k}{\tau T_0}\right)\right|^2. \tag{83}$$

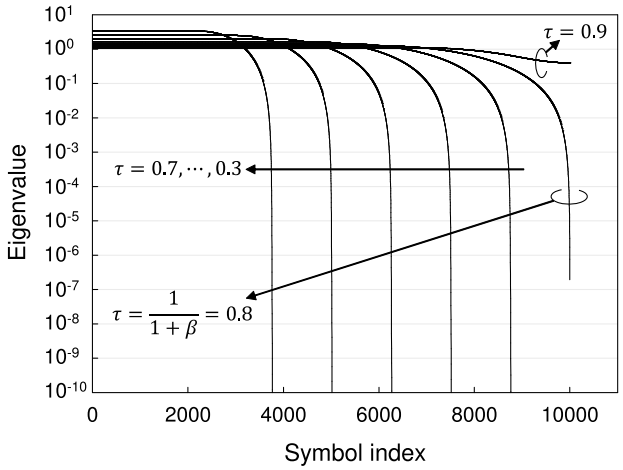

FIGURE 10. The eigenvalue distribution of **G**, where the block size was set to $N = 10000$. The roll-off factor was set to $\beta = 0.25$, while the symbol packing ratio was set to $\tau = 0.9, 0.8, 0.7, 0.6, 0.5, 0.4$, and 0.3.

Since $H_{\rm fo}(f)$ includes spectral nulls when $\tau < 1/(1+\beta)$, the matrix **G** may have quite low eigenvalues, depending on τ and β [14]. Fig. 10 shows the distribution of the eigenvalues λ_k for a block size of $N = 10,000$, where the roll-off factor was given by $\beta = 0.25$, and the symbol packing ratio was set to $\tau = 0.9, 0.8, 0.7, 0.6, 0.5, 0.4$, and 0.3. As shown in Fig. 10, when $\tau < 1/(1+\beta)$, the partial eigenvalues of the matrix **G** were too low to be calculated in a standard double-precision environment. Hence, the substreams corresponding to such low eigenvalues may suffer from poor detection performance. Note that for a finite block length N, the matrix **G** is guaranteed to be positive definite, hence all eigenvalues λ_k are non-zero [14].

In order to mitigate the detrimental effects of extremely low eigenvalues, in [45] an adaptive bit-loading scheme was developed for EVD-precoded FTN signaling. In this scheme, the information bits are assigned to streams by ensuring that the MED is increased, where the substream associated with extremely low eigenvalue may be deactivated (truncated). Furthermore, motivated by the classic waterfilling algorithm developed for an SVD-precoded spatial multiplexing MIMO system, in [15] both the optimal and a truncated power allocation schemes were proposed for EVD-precoded FTN signaling, in order to increase the achievable information rate. The corresponding system model and information-theoretic analysis will be presented in detail in Section VIII.

C. INVERSE SQUARE ROOT PRECODING OF FTN SIGNALING

In [13], Gattami *et al.* presented a TPC scheme relying on the inverse square root (ISR) of the ISI matrix **G**. Since the ISI matrix **G** is positive definite, the existence of a unique square root matrix $\mathbf{G}^{\frac{1}{2}}$ satisfying the relationship $\mathbf{G} = \mathbf{G}^{\frac{1}{2}}\mathbf{G}^{\frac{1}{2}}$ is guaranteed [13]. Hence, by setting the TPC matrix to $\mathbf{F} = \mathbf{G}^{-\frac{1}{2}}$ and the weight matrix to $\mathbf{W} = \mathbf{G}^{-\frac{1}{2}}$, the received signals are diagonalized as follows:

$$\mathbf{r}_d = \mathbf{G}^{-\frac{1}{2}}\mathbf{G}\mathbf{G}^{-\frac{1}{2}}\mathbf{s} + \mathbf{G}^{-\frac{1}{2}}\boldsymbol{\eta} \tag{84}$$

$$= \mathbf{s} + \boldsymbol{\eta}_g, \tag{85}$$

where we have $\boldsymbol{\eta}_g = \mathbf{G}^{-\frac{1}{2}}\boldsymbol{\eta}$. The covariance matrix of $\boldsymbol{\eta}_g$ is given by $\mathbb{E}[\boldsymbol{\eta}_g\boldsymbol{\eta}_g^H] = N_0\mathbf{I}_N$, and hence the associated noises are uncorrelated. The ISR-based TPC allows us to carry out low-complexity symbol-by-symbol demodulation, similar to the EVD-precoded FTN signaling of Section VII-B. A further point to note is that the square root of **G** is represented by using EVD as follows: $\mathbf{G}^{\frac{1}{2}} = \mathbf{V}\Lambda^{\frac{1}{2}}\mathbf{V}^T$. Hence, its inverse is given by $\mathbf{G}^{-\frac{1}{2}} = \mathbf{V}\Lambda^{-\frac{1}{2}}\mathbf{V}^T$.

BER comparisons between uncoded EVD-precoded FTN signaling and ISR-precoded FTN signaling can be found in [44], [45], [134].

D. TOMLINSON-HARASHIMA PRECODING-AIDED FTN SIGNALING

In contrast to the linear-precoding-aided FTN signaling of [13]–[15], [44], [45], [134], non-linear Tomlinson-Harashima precoding (THP) was exploited for FTN signaling in [47], [48], [133], [133]–[141]. The first THP-aided FTN signaling scheme was proposed in [47], based on the spectral factorization formulated as $G(z) = D(z)D^*(1/z^*)$, where $G(z)$ represents the z-transform of the τT_0-spaced samples of $g(t)$ [47]. In order to further improve the detection performance attained, linear pre-equalization (LPE) was introduced into THP-aided FTN signaling. The BER results of an LDPC-encoded coherent optical channel showed that an ISI-free performance bound was achievable for $\tau = 0.85$ and $\tau = 0.8$ using QPSK modulation and $\beta = 0.3$. Moreover, in [130], the LPE-aided THP-FTN signaling scheme was extended to one supporting dual-polarized FTN signaling. However, since the spectral factorization of $G(z)$ is infeasible when the folded pulse spectrum (83) has spectral nulls [22], [47], the symbol packing ratio τ was restricted to the range of $[1/(1+\beta), 1]$ in [47], [130]. Moreover, it was revealed in [48] that significant residual ISI is encountered in THP-FTN signaling, albeit its detrimental effects may be mitigated by SIC at the receiver. In [133], THP-based FTN signaling was proposed for a single-mode fiber optical communication channel.

E. PRECODING-INDUCED SPECTRUM BROADENING

It was pointed out in [129] that the precoded FTN signaling schemes may result in the broadening of the transmit signal's spectrum. In [129], the power spectral density (PSD) of precoded FTN signaling was investigated and it was shown that spectrum broadening is not imposed if and only if the associated signaling pulse employed is strictly bandlimited. Hence, the precoded FTN signaling scheme relying on an RRC shaping filter does not broaden the associated spectrum, since the RRC pulse is strictly bandlimited to the frequency range of $[-(1+\beta)W, (1+\beta)W]$. However, since an ideal

TABLE 8. Information-theoretic analyses of unprecoded FTN signaling and their contributions.

Year	Authors	Contribution	Channel
2009	Rusek and Anderson [5]	Derived the capacity of unprecoded FTN signaling in a rigorous manner for the first time, revealing that when employing an RRC shaping filter having a roll-off factor of $\beta > 0$, i.e., a shaping filter with excess bandwidth, FTN signaling achieves a higher capacity than classic Nyquist signaling.	AWGN
2010	Yoo and Cho [6]	Demonstrated that when $\tau \to 0$, binary unprecoded FTN signaling has the potential to attain an information rate close to the capacity derived in [5].	AWGN
2013	Modenini *et al.* [7]	Presented a design guideline of a shaping filter that improves a constrained information rate of FTN signaling, which is modeled as a special case of an ISI channel.	AWGN
2014	Hefnawy and Kramer [8]	Analyzed the capacity of FTN signaling in the scenario of a spectrum sharing system.	AWGN
	Modenini *et al.* [135]	Showed a capacity gain of FTN signaling over Nyquist signaling in a measured large-scale MISO channel, where the base station was equipped with 128 antenna elements.	Frequency-selective
2015	Feng and Bajcsy [9]	Investigated the capacity of FTN signaling over a multiple-access channel.	AWGN
	Yuhas *et al.* [136]	Evaluated the information rate of FTN signaling over a MIMO channel with receiver-side CSI, where a non-bandlimited rectangular shaping filter was considered.	Frequency-flat
2016	Kim *et al.* [10]	Considered the multi-user FTN signaling scenario, and derived the capacity in an AWGN channel. The achievable performance gain of the proposed scheme over Nyquist signaling counterpart was demonstrated for equal and unequal power allocation to users.	AWGN
2017	Bogale *et al.* [11]	Investigated the capacity of FTN signaling over a frequency-selective SIMO channel.	Frequency-selective

bandlimited shaping filter having an infinite IR is not implementable in practice, we may have to check the PSD of precoded FTN signaling [129].

VIII. INFORMATION-THEORETIC ANALYSIS OF FTN SIGNALING

This section analyzes FTN signaling from an information-theoretic perspective by providing comprehensive comparisons of the information rate improvements attained over conventional Nyquist signaling.

Classically, capacity was defined as the achievable upper bound of the information rate [142]. More specifically, in a bandlimited complex-valued AWGN channel having a bandwidth of $2W$ [Hz] and noise variance N_0, the capacity of Nyquist signaling having $\mathbb{E}[|s_k|^2] = \sigma_s^2$ is formulated as

$$C = 2W \log_2 \left(1 + \frac{\sigma_s^2}{N_0}\right) \quad \text{[bits/sec]}. \tag{86}$$

The capacity of FTN signaling was derived for several scenarios, revealing the achievable gain of FTN signaling over its Nyquist signaling counterpart. Here, we consider three FTN signaling scenarios, namely, unprecoded FTN signaling [5], [6], [8]–[11], [135], [136], FTN signaling relying on FD filtering [12], [131], [143], [144], and precoded FTN signaling [13]–[15], [17]. The related literature is summarized in Tables 8, 9, and 10, respectively.

A. UNPRECODED FTN SIGNALING

The first information-theoretic analysis of FTN signaling was presented by Rusek and Anderson in [5], where the capacity of unprecoded FTN signaling in an AWGN channel was derived by extending the classic capacity of Nyquist signaling over an ISI channel, as follows [5]:

$$C^{\text{FTN}} = \int_{-1/(2\tau T_0)}^{1/(2\tau T_0)} \log_2 \left(1 + \frac{\sigma_s^2}{N_0} H_{\text{fo}}(f)\right) df \ \text{[bits/sec]}, \tag{87}$$

where $H_{\text{fo}}(f)$ is the folded signaling pulse spectrum defined by (83). Furthermore, the complex-valued independent and identically distributed Gaussian symbol is assumed. For $\tau = 1$, the capacity formula (87) coincides with that of its Nyquist signaling counterpart (86). The capacity, normalized by the bandwidth of the RRC shaping filter having a roll-off factor β [5], is formulated by

$$R^{\text{FTN}} = \frac{C^{\text{FTN}}}{2(1+\beta)W} \quad \text{[bps/Hz]}, \tag{88}$$

In [5], Rusek and Anderson showed that when employing an RRC shaping filter, the capacity of unprecoded FTN signaling (87) becomes higher than that of its classic Nyquist signaling counterpart (86) employing the same RRC shaping filter. However, when employing the ideal rectangular shaping filter ($\beta = 0$), no performance gain is obtained by FTN signaling in terms of bandwidth efficiency. This implies that the bandwidth efficiency benefits of unprecoded FTN signaling are attainable owing to an excess bandwidth, which cannot be exploited in the conventional Nyquist signaling scheme.

Fig. 11 shows the normalized capacity (88) of unprecoded FTN signaling, where an RRC filter having a roll-off factor β was used both for unprecoded FTN signaling and for Nyquist signaling. The symbol packing ratio was varied from $\tau = 0.9$ to 0.1 in steps of 0.1, and the roll-off factor was set to $\beta = 0, 0.22, 0.5,$ and 1 in Figs. 11(a), 11(b), 11(c), and 11(d), respectively. For the sake of normalization, we assumed that the Nyquist symbol interval was $T_0 = 1$ sec, and the corresponding bandwidth was given by $2W = 1$ Hz. The SNR was defined by σ_s^2/N_0 dB. Observe in Fig. 11(a) that when the sinc signaling pulse ($\beta = 0$) was employed, FTN signaling did not achieve any capacity gain over conventional Nyquist signaling. However, as shown in Figs. 11(b), 11(c), and 11(d), the FTN signaling achieved higher capacity than its Nyquist signaling counterpart employing the same RRC shaping filter owing to the capability of exploiting the excess bandwidth. Upon increasing β, the capacity gain of FTN signaling over Nyquist signaling monotonically increased.

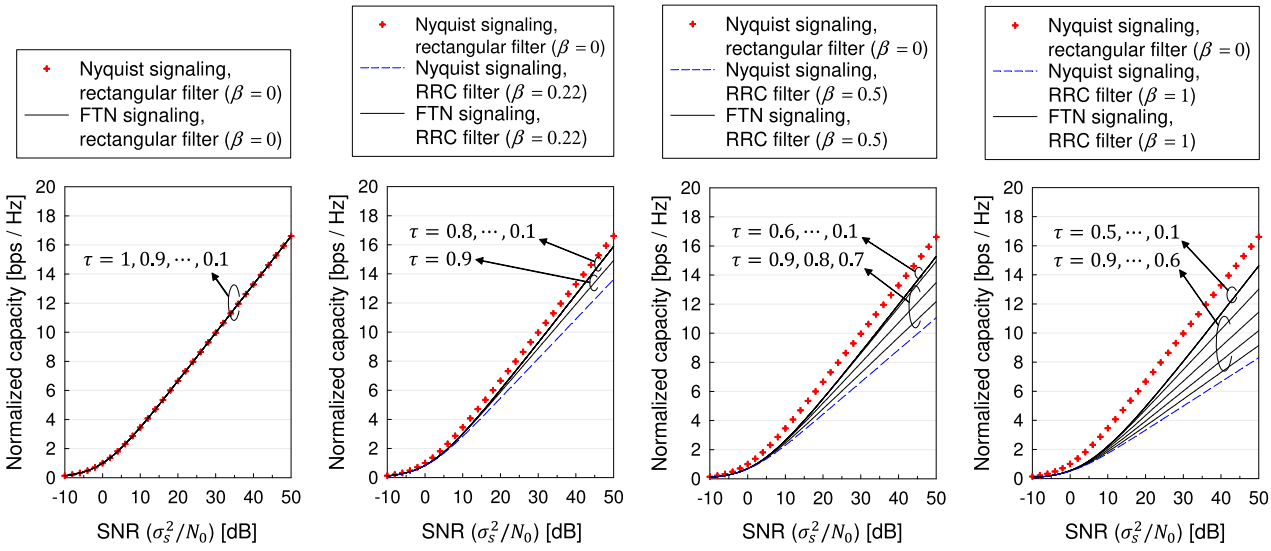

(a) Rectangular filter, $\beta = 0$. (b) RRC filter, $\beta = 0.22$. (c) RRC filter, $\beta = 0.5$. (d) RRC filter, $\beta = 1$.

FIGURE 11. Capacities C^{FTN} and C of FTN signaling and classic Nyquist signaling ($\tau = 1$), where an RRC shaping filter having roll-off factor β was employed. The symbol packing ratio of FTN signaling was varied from $\tau = 0.9$ to 0.1 in steps of 0.1. The roll-off factor was set to (a) $\beta = 0$, (b) $\beta = 0.22$, (c) $\beta = 0.5$, and (d) $\beta = 1$. The symbol interval satisfying the Nyquist criterion was fixed as $T_0 = 1$ sec.

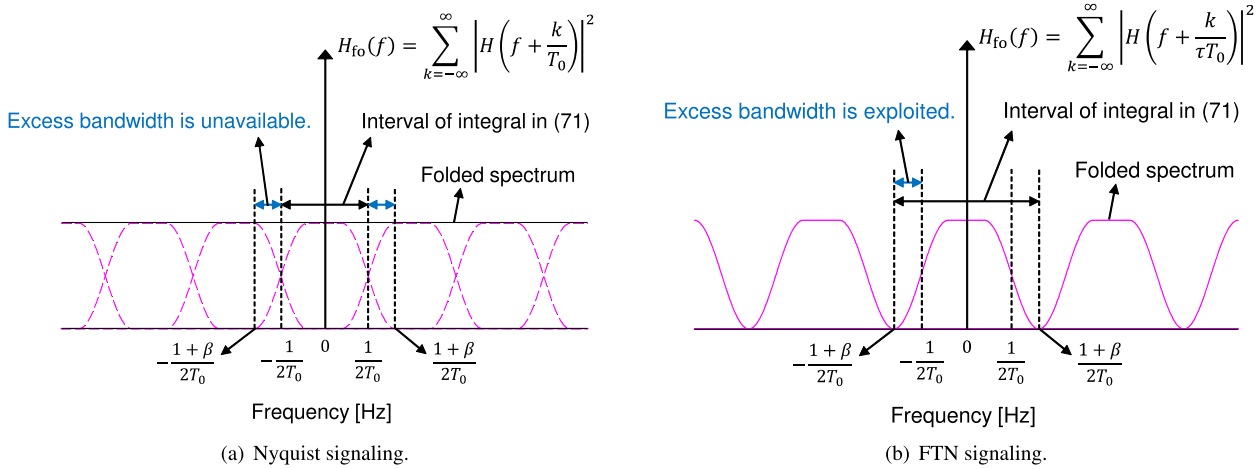

(a) Nyquist signaling. (b) FTN signaling.

FIGURE 12. The fundamental benefits of FTN signaling over classic Nyquist signaling, which are achievable owing to the exploitation of the excess bandwidth attained. An RRC shaping filter having the roll-off factor of $\beta = 0.6$ and the symbol packing ratio of $\tau = 1/(1+\beta) = 0.625$ were assumed.

More specifically, the highest capacity was achieved at $\tau = 0.8$, 0.6, and 0.5 for the scenarios of $\beta = 0.22$, 0.5, and 1, respectively. However, further reducing τ did not yield any additional capacity gain. Moreover, the normalized capacity of FTN signaling employing an RRC shaping filter ($\beta > 0$) was lower than that of Nyquist signaling employing the ideal rectangular shaping filter having $\beta = 0$. Fig. 12 illustrates the fundamental benefits of FTN signaling over classic Nyquist signaling, which is achievable owing to the exploitation of the excess bandwidth. We assumed using an RRC shaping filter having the roll-off factor of $\beta = 0.6$ and the symbol packing ratio of $\tau = 1/(1+\beta) = 0.625$. The FTN signaling scheme achieves a higher capacity than its Nyquist signaling counterpart employing the same RRC shaping filter due to exploiting the resultant excess bandwidth. Further reducing τ below $1/(1+\beta)$ does not lead to any additional capacity gain, since the folded pulse spectrum $H_{fo}(f)$ includes spectral nulls when $\tau < 1/(1+\beta)$ [5].

To elaborate a little further, in Fig. 13 we show the normalized capacity of unprecoded FTN signaling for each τ value for SNRs of 30 dB and 60 dB. The symbol packing ratio was varied from $\tau = 1$ to 0.4 in steps of 0.02. The other system parameters were the same as those used in Fig. 11. As shown in Fig. 13, the capacities of unprecoded FTN signaling using the roll-off factors of $\beta = 0.22$, 0.5, and 1 were highest for $\tau \leq 0.82$, 0.66, and 0.5, respectively. This confirmed that

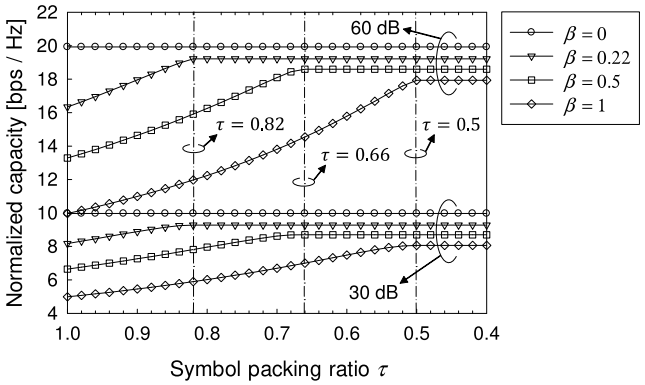

FIGURE 13. Capacity C^{FTN} of FTN signaling for each τ value for the SNRs of 30 dB and 60 dB. The symbol packing ratio was varied from $\tau = 1$ to 0.4 in steps of 0.02, while the roll-off factor was set to $\beta = 0$, 0.22, 0.5, and 1.

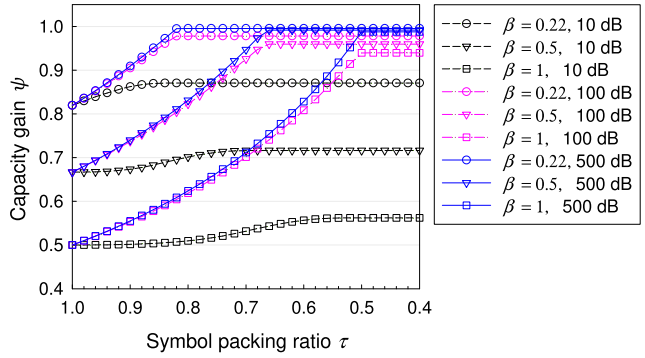

FIGURE 14. Capacity gain ψ for the SNRs of 10 dB, 100 dB, and 500 dB. The symbol packing ratio was varied from $\tau = 1$ to 0.4 in steps of 0.02, while the roll-off factor was set to $\beta = 0.22$, 0.5, and 1.

the achievable capacity gain of unprecoded FTN signaling is upper-bounded by $\tau = 1/(1+\beta)$, which corresponds to the excess bandwidth of the RRC shaping filter.

Furthermore, the capacity gain of FTN signaling employing an RRC shaping filter over Nyquist signaling employing the ideal rectangular shaping filter is defined by [5]

$$\psi = \frac{R^{\mathrm{FTN}}}{C/2W}. \tag{89}$$

In [5], Rusek and Anderson proved that the capacity gain (89) approaches 1 when $\sigma_s^2/N_0 \to \infty$. Fig. 14 shows ψ (89) for the SNRs of 10 dB, 100 dB, and 500 dB. The symbol packing ratio and the roll-off factor were the same as those used in Fig. 13. As seen from Fig. 14, the capacity gain ψ for $\tau \leq 1/(1+\beta)$ approached 1 at the extreme SNR of 500 dB. Hence, unprecoded FTN signaling employing an RRC shaping filter approaches but does not outperform the Nyquist signaling employing the ideal sinc signaling pulse.

In [6], the information rate of binary FTN signaling was investigated; it was shown that when $\tau \to 0$, binary FTN signaling is capable of attaining an information rate close to the capacity of unprecoded FTN signaling C^{FTN} derived in [5]. Furthermore, the information rate of unprecoded FTN signaling has been studied in a multi-user scenario [8]–[10]. In [10], FTN signaling was considered in a multi-user downlink scenario, where the different user's data symbols were broadcast by superimposing multiple different FTN signals. The associated capacity was derived, and the presented scheme's performance gain over its Nyquist signaling counterpart was quantified.

Although most of the capacity expression of unprecoded FTN signaling were derived for an AWGN channel [5], [6], [8]–[10], those of a frequency-flat MIMO channel and of a frequency-selective single-input multiple-output (SIMO) channel were quantified in [136], [145] and [11], respectively, assuming having perfect receiver-side CSI. Moreover, in [135], the capacity of FTN signaling was calculated based on a measured large-scale multiple-input single-output (MISO) channel, where the base station employed 128 antenna elements.

B. FTN SIGNALING RELYING ON FD FILTERING

To further increase the information rate, an FD filter was invoked in unprecoded FTN signaling [12], [143], [144].

In [143], the classical waterfilling algorithm was used for FTN signaling, where the PSD of transmit signals was reshaped by filtering for ensuring that the information rate was maximized under a specific average power constraint. However, almost no performance improvement was achieved when a practical RRC shaping filter was employed.

As shown in Fig. 14, unprecoded FTN signaling [5] using an RRC shaping filter ($\beta > 0$) achieved a normalized capacity close to that of its Nyquist signaling bound when using a rectangular shaping filter, i.e., $\psi \simeq 1$, at sufficiently high SNRs. However, at low SNRs, a non-negligible capacity gap was found between the two schemes. To reduce the capacity gap, in [144], Hefnawy *et al.* designed an FD filter based on the Lagrange multiplier method. As a result, a higher information rate than unprecoded FTN signaling in [5] was achieved. Furthermore, spectral shaping similar to [144] was used in [12], where both AWGN and frequency-selective fading channels were considered.

In [131], the information rate of FTN signaling using QAM was investigated, where the signaling pulse of an RRC filter was truncated to reshape the spectrum with the aid of particle swarm optimization under the constraint of a specific maximum out-of-band emission. Both analytical performance results, as well as simulation-based BER performance results were reported for a multi-stage-concatenated channel-coded system. It was demonstrated that the FTN signaling scheme using a time-truncated signaling pulse, 4-QAM and $\tau = 0.25$, exhibited a BER advantage over its Nyquist signaling counterpart employing 256-QAM.

C. PRECODED FTN SIGNALING

In [14], the capacity of EVD-precoded FTN signaling was derived. More specifically, based on the approximation of (82), the capacity of EVD-precoded FTN signaling is

TABLE 9. Information-theoretic analysis of FTN signaling with frequency-domain filtering and their contributions.

Year	Authors	Contribution	Channel
2011	Kim and Bajcsy [143]	Evaluated the capacity of cyclostationary FTN signaling, employing the RRC shaping filter. The waterfilling algorithm was exploited for FD filtering, which is used for increasing the information rate, where a limited performance gain over Nyquist signaling was reported for a two-path fading channel.	Frequency-selective
2014	Hefnawy *et al.* [144]	Designed an FD filter to improve the achievable information rate of FTN signaling, with the aid of the Lagrange multiplier method.	AWGN
2019	Che *et al.* [131]	Investigated a constrained information rate of FTN signaling, employing L-point QAM. The time-truncated pulse of an RRC shaping filter was designed such that the constrained information rate was maximized, based on the particle swarm optimization algorithm.	AWGN
2020	Ganji *et al.* [12]	Presented the design guideline of an FD filter to increase the information rate of FTN signaling both for the AWGN and frequency-selective fading scenarios, based on the Lagrange multiplier method.	AWGN and frequency-selective

formulated as follows [14]:

$$C_{\mathrm{EVD}}^{\mathrm{FTN}} = \int_{-1/(2\tau T_0)}^{1/(2\tau T_0)} \log_2\left(1+\frac{\sigma_s^2}{N_0}H_{\mathrm{fo}}(f)\right) df \tag{90}$$

$$= C^{\mathrm{FTN}}. \tag{91}$$

As shown in (91), the capacity of EVD-precoded FTN signaling is consistent with that of unprecoded FTN signaling of (87). Hence, EVD-precoded FTN signaling does not yield any information-rate gain over its unprecoded counterpart [14], [15].

To overcome this limitation, EVD-precoded FTN signaling combined with power allocation was proposed in [15]. More specifically, motivated by the classic waterfilling algorithm conceived for an SVD-precoded spatial-multiplexing MIMO system [56], in [15], both optimal and truncated power allocation schemes were developed for increasing the achievable information rate of EVD-precoded FTN signaling. In [15], the precoding matrix was set to $\mathbf{F} = \mathbf{V}\Gamma$, where Γ is a diagonal matrix having the diagonal elements of $[\sqrt{\gamma_0}, \cdots, \sqrt{\gamma_{N-1}}]$. The received signals of EVD-precoded FTN signaling are decoupled to parallel streams with diagonalization, and mutual information of EVD-precoded FTN signaling with power allocation is formulated as [15]

$$I(\mathbf{s};\mathbf{r}_d) \leq \sum_{k=0}^{N-1} \log_2\left(1+\frac{\lambda_k\gamma_k\sigma_s^2}{N_0}\right), \tag{92}$$

under the assumption of complex-valued Gaussian symbol transmission. The associated capacity is obtained by assuming an infinite channel code length as follows [15]:

$$C_{\mathrm{opt}}^{\mathrm{FTN}} = \lim_{N\to\infty} \frac{1}{N\tau T_0} \sum_{k=0}^{N-1} \log_2\left(1+\frac{\lambda_k\gamma_k\sigma_s^2}{N_0}\right). \tag{93}$$

Moreover, the average transmit energy $\tilde{E}_p$ of EVD-precoded FTN signaling combined with power allocation is expressed as:

$$\tilde{E}_p = \mathbb{E}\left[\mathbf{s}^H\mathbf{\Gamma}\mathbf{V}^T\mathbf{G}\mathbf{V}\mathbf{\Gamma}\mathbf{s}\right] \tag{94}$$

$$= \sigma_s^2 \sum_{k=0}^{N-1} \lambda_k\gamma_k. \tag{95}$$

In [15], based on the Lagrange multiplier method under the energy constraint of $\tilde{E}_p = E_p$, the coefficients γ_k were optimized for ensuring that the mutual information (92) was maximized. The associated Lagrange function is given by

$$J = \sum_{k=0}^{N-1} \log_2\left(1+\frac{\lambda_k\gamma_k\sigma_s^2}{N_0}\right) - \alpha\left(\sum_{k=0}^{N-1}\lambda_k\gamma_k - N\right),$$

where α represents the Lagrange multiplier. By solving the optimization problem of $\partial J/\partial\gamma_k = 0$ subject to $\gamma_k \geq 0$, the optimized coefficients γ_k are as follows:

$$\gamma_k = \frac{1}{\lambda_k} \quad \text{for} \quad k = 0, \cdots, N-1. \tag{96}$$

Note that the constraint $\gamma_k \geq 0$ is always satisfied for all the substreams [15].[2] Hence, the TPC matrix that maximizes the information rate achieved by EVD-precoded FTN signaling is given by $\mathbf{F} = \mathbf{V}\Gamma = \mathbf{V}\Lambda^{-\frac{1}{2}}$. The associated received signal model is given by

$$\mathbf{r}_d = \Lambda^{\frac{1}{2}}\mathbf{s} + \boldsymbol{\eta}_v, \tag{97}$$

where the SNRs of all the N substream in (97) are identical, since $\mathbb{E}[\boldsymbol{\eta}_v\boldsymbol{\eta}_v^H] = N_0\mathbf{\Lambda}$. Note that in [14], when the folded pulse spectrum (83) includes spectral nulls, i.e., when $\tau < 1/(1+\beta)$, the subset of the eigenvalues λ_k approaches zero, as the block size N goes to infinity. Since the optimal coefficients γ_k of (96) associated with the asymptotically zero eigenvalues cannot be defined, the associated substreams have to be deactivated in order to correctly generate the FTN signal for $\tau < 1/(1+\beta)$.[3] By contrast, for $\tau \geq 1/(1+\beta)$, the folded spectrum does not include spectral nulls, and hence all the eigenvalues are positive. Hence, for $\tau \geq 1/(1+\beta)$, the capacity of EVD-precoded FTN signaling with optimal

[2] In the conventional SVD-precoded MIMO transmission scheme based on the waterfilling algorithm [56], some of the available substreams are truncated in order to maximize the associated information rate under a given power constraint. By contrast, in EVD-precoded FTN signaling with optimal power allocation, truncation is not imposed, and all of the N parallel substreams are used for data transmission.

[3] In [15], under the idealistic assumption that all the eigenvalues are positive even for $N \to \infty$, the capacity of EVD-precoded FTN signaling with power allocation was formulated.

TABLE 10. Information-theoretic analyses of precoded FTN signaling and Their Contributions.

Year	Authors	Contribution	Channel
2013	Kim [146]	Designed a precoding matrix, where the precoded symbols $\mathbf{x} = \mathbf{Fs}$ has covariance matrix $\mathbb{E}[\mathbf{x}\mathbf{x}^H] = \sigma_s^2\mathbf{G}^{-1}$, in order to maximize the information rate of FTN signaling in an AWGN channel.	AWGN and frequency-selective
2015	Gattami *et al.* [13]	Conceived precoding of the square root of the FTN-induced ISI matrix and derived the associated capacity.	AWGN
2016	Kim [14]	Derived the capacity of precoded FTN signaling based on EVD of the ISI matrix. The derived capacity agreed with that of the unprecoded FTN signaling of [5].	AWGN
2019	Ishihara and Sugiura [15]	Proposed EVD-precoded FTN signaling combined with optimal and truncated power allocation. Information-theoretic performance analyses showed that a higher information rate than unprecoded FTN signaling and Nyquist signaling was achievable by EVD-precoded FTN signaling combined with power allocation, when a practical RRC shaping filter was employed.	AWGN
2020	K. Masaki *et al.* [16]	Evaluated the effects of the eigenvalue distribution of ISI matrix $\mathbf{G}$ on the achievable information rate of EVD-precoded FTN signaling combined with truncated power allocation of [15]. The tradeoff between the information rate and the calculation precision was demonstrated, with the aid of multiple-precision floating-point number calculations.	AWGN
2021	Mohammadkarimi *et al.* [17]	Analyzed the achievable information rate of FTN signaling with a finite code length, showing that FTN signaling achieved a higher information rate than Nyquist signaling using the same finite code length.	AWGN
	Ishihara and Sugiura [18]	Extended EVD-precoded FTN signaling combined with optimal power allocation assuming an AWGN channel [15] to that supporting a frequency-selective fading channel, which was capable of achieving an information rate close to the ideal rectangular-filter bound, while employing a practical RRC shaping filter.	Frequency-selective

power allocation is given by substituting (96) into (93) as follows [13], [15], [146]:

$$C_{\text{opt}}^{\text{FTN}} = \lim_{N\to\infty} \frac{1}{N\tau T_0} \sum_{k=0}^{N-1} \log_2\left(1 + \frac{\sigma_s^2}{N_0}\right) \tag{98}$$

$$= \frac{2W}{\tau} \log_2\left(1 + \frac{\sigma_s^2}{N_0}\right) \text{ [bits/sec]}, \tag{99}$$

where we had $T_0 = 1/(2W)$. For $\tau = 1$, the metric (99) matches the capacity formula of conventional Nyquist signaling in (86). The associated normalized capacity is defined by

$$R_{\text{opt}}^{\text{FTN}} = \frac{C_{\text{opt}}^{\text{FTN}}}{2(1+\beta)W} \text{ [bps/Hz]}. \tag{100}$$

Moreover, when $\tau = 1/(1+\beta)$, the normalized capacity (100) becomes

$$R_{\text{opt}}^{\text{FTN}} = \log_2\left(1 + \frac{\sigma_s^2}{N_0}\right) \text{ [bps/Hz]}. \tag{101}$$

This normalized capacity in (101) corresponds to that of the Nyquist-criterion-based system employing the sinc signaling pulses having the rectangular frequency support of $[-W, W]$.

Fig. 15 shows the normalized capacity (100) of EVD-precoded FTN signaling combined with optimal power allocation, employing an RRC shaping filter having the roll-off factor of $\beta = 0.25$, while the symbol packing ratio was set to $\tau = 1/(1+\beta) = 0.8$. The normalized capacities of the Nyquist signaling scheme ($\tau = 1$) and the unprecoded FTN signaling scheme with $\tau = 0.8$ were plotted as the benchmarks, where both the schemes employed the same RRC shaping filter as that used by the EVD-precoded FTN signaling scheme. Moreover, the Shannon capacity assuming

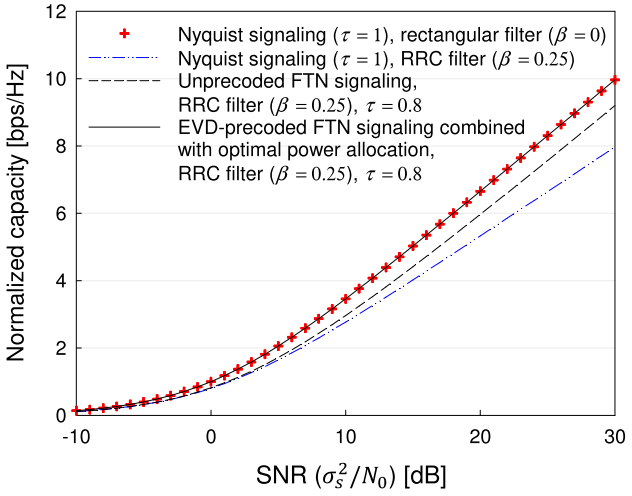

FIGURE 15. Normalized capacity (100) of EVD-precoded FTN signaling combined with optimal power allocation. The roll-off factor was set to $\beta = 0.25$, while the symbol packing ratio was set to $\tau = 1/(1+\beta) = 0.8$.

the use of the ideal rectangular shaping filter of $\beta = 0$ was also shown. Observe in Fig. 15 that EVD-precoded FTN signaling combined with optimal power allocation achieved the capacity bound assuming the ideal rectangular shaping filter ($\beta = 0$) while outperforming the capacity of the corresponding Nyquist signaling scheme using a practical RRC shaping filter having $\beta > 0$. Hence, EVD-precoded FTN signaling combined with optimal power allocation is capable of fully exploiting the excess bandwidth of an RRC shaping filter, while Nyquist signaling and unprecoded FTN signaling using an RRC shaping filter are not.

Note that in the earlier study of [13], Gattami *et al.* investigated the information rate of precoded FTN signaling with the aid of the ISR-based TPC matrix of $\mathbf{G}^{-\frac{1}{2}} = \mathbf{V}\Lambda^{-\frac{1}{2}}\mathbf{V}^T$,

and the capacity derived was the same as in (99). Moreover, in the Ph.D. thesis of Kim in 2013 [146], it was shown that if the TPC matrix $\mathbf{F}$ is designed for ensuring that the covariance matrix of the precoded symbols $\mathbf{x}$ becomes $\mathbb{E}[\mathbf{x}\mathbf{x}^H] = \mathbb{E}[\mathbf{F}\mathbf{s}\mathbf{s}^H\mathbf{F}^H] = \sigma_s^2\mathbf{G}^{-1}$, the information rate achieved by FTN signaling is maximized. The corresponding capacity was formulated as (99). The TPC matrices $\mathbf{G}^{-\frac{1}{2}}$ and $\mathbf{V}\Lambda^{-\frac{1}{2}}$ advocated in [13] and [15], respectively, result in such a covariance matrix [146]. Hence, these TPC matrices were optimal in terms of the achievable information rate [146]. Most recently, the concept of EVD-precoded FTN signaling combined with power allocation was extended to the scenario of NOFDM in [85]. It was demonstrated in [85] that the EVD-precoded NOFDM scheme combined with power allocation is capable of achieving a higher capacity than the conventional OFDM scheme.

It is worth mentioning that the optimal power allocation of (96) designed for EVD-precoded FTN signaling is not the classic water-filling solution, while it was the water-filling solution for the SVD-precoded spatial-multiplexing MIMO system. More specifically, in the conventional SVD-precoded MIMO system, a higher power is allocated to the active substreams associated with higher singular values, while the remaining substreams may be deactivated. As a result, the optimal power allocation is reminiscent of waterfilling [56]. By contrast, in the EVD-precoded FTN signaling scheme combined with optimal power allocation, non-zero power is allocated to each substream for ensuring that all N substreams have an identical equivalent SNR of σ_s^2/N_0, as shown in (97); explicitly, this is not waterfilling.

Furthermore, in [18], EVD-precoded FTN signaling combined with optimal power allocation [15] was extended to that supporting a frequency-selective fading channel, which achieves an information rate close to the ideal rectangular-filter bound in dispersive channels.[4]

D. NUMERICAL ILL-CONDITIONING CAUSED BY EXTREMELY LOW EIGENVALUES

As mentioned in Section VIII-C, for an infinite channel code length, optimal power allocation (96) is only possible in the range of $\tau \geq 1/(1+\beta)$ and the associated capacity is given by (99). However, it was proved in [14] that for finite N, the ISI matrix $\mathbf{G}$ is always positive definite regardless of the values of τ and β. Thus, for finite N, EVD-precoded FTN signaling combined with optimal power allocation is theoretically implementable even in the high-rate scenarios of $\tau < 1/(1+\beta)$.[5]

However, in a low-τ scenario, EVD-precoded FTN signaling combined with optimal power allocation suffers from numerical ill-conditioning due to the presence of extremely low eigenvalues of the ISI matrix, when $\tau < 1/(1+\beta)$.[6] Since the TPC matrix $\mathbf{F} = \mathbf{V}\Lambda^{-\frac{1}{2}}$ of EVD-precoded FTN signaling combined with optimal power allocation requires the reciprocals of the eigenvalues, its numerical computations become ill-conditioned in a low-τ scenario.[7] The TPC matrix $\mathbf{G}^{-\frac{1}{2}} = \mathbf{V}\Lambda^{-\frac{1}{2}}\mathbf{V}^T$ contains the reciprocals of the eigenvalues, hence it also suffers from the same ill-conditioning problem. Note that as shown in Fig. 10, when $\tau \geq 1/(1+\beta)$, the ISI matrix $\mathbf{G}$ has no extremely low eigenvalues. Hence the associated matrix inversions are accurately computed in the standard double-precision environment.

E. EVD-PRECODED FTN SIGNALING RELYING ON TRUNCATED POWER ALLOCATION

To solve the above-mentioned numerical ill-conditioning problem, suboptimal truncated power allocation was proposed for the first time in [15]. More specifically, in [15], the optimal power allocation of (96) was modified to

$$\gamma_k = \begin{cases} \dfrac{1}{\lambda_k} \cdot \dfrac{N}{M} & (\lambda_k \geq t_h) \\ 0 & (\lambda_k < t_h), \end{cases} \tag{102}$$

where t_h represents a threshold value. The M out of N substreams satisfying the condition of $\lambda_k \geq t_h$ are used for data transmission, while the remaining $(N-M)$ substreams are deactivated. Hence, truncated power allocation of (102) allows us to dispense with the reciprocals of the extremely low eigenvalues [15]. The coefficient N/M in (102) is required to satisfy the energy constraint of $\tilde{E}_p = E_p$.

In [16], the effects of the eigenvalue distribution on the achievable information rate were further explored. More specifically, the eigenvalue decomposition of $\mathbf{G}$ was carried out based on the multiple-precision floating-point arithmetic library of [150] that enables more precise computation than the standard double-precision environment.

F. EFFECTS OF IBI ON INFORMATION RATE

The detrimental IBI effects were ignored in the previous FTN studies by assuming single block based transmissions in FTN signaling. To provide further insights, we include Figs. 16(a) and 16(b) for providing examples of the baseband transmit signals $x(t)$ of the EVD-precoded FTN signaling schemes without power allocation and with truncated power allocation, respectively. We employed the system parameters of $\tau = 0.1, \beta = 0.22$, and $N = 1,000$. Moreover,

[4] In [146], a similar precoded FTN signaling system was presented, but no analytical and numerical performance results were provided.

[5] To rigorously analyze the information rate for a finite code length, the effects of the non-zero block error has to be considered [147]. In [17], the achievable information rate of FTN signaling for a finite code length was analyzed, showing that FTN signaling outperforms its Nyquist signaling counterpart at the same finite code length.

[6] In [14]–[16], [146], it was mentioned that the FTN-induced ISI matrix $\mathbf{G}$ based on the sinc filter is known as a prolate matrix [148], [149]. A prolate matrix with large N typically has extremely low eigenvalues, and hence the computation of its inverse is numerically ill-conditioned [148], [149].

[7] In our additional simulations, it was observed that for low τ, the average energy of the transmit EVD-precoded FTN signals with optimal power allocation did not match its theoretical value, where we carried out the associated computations based on standard double-precision floating-point numbers. This is because the precoding matrix $\mathbf{V}\Lambda^{-\frac{1}{2}}$ and the corresponding transmit signals $x(t)$ were not precisely computed due to the presence of extremely low eigenvalues.

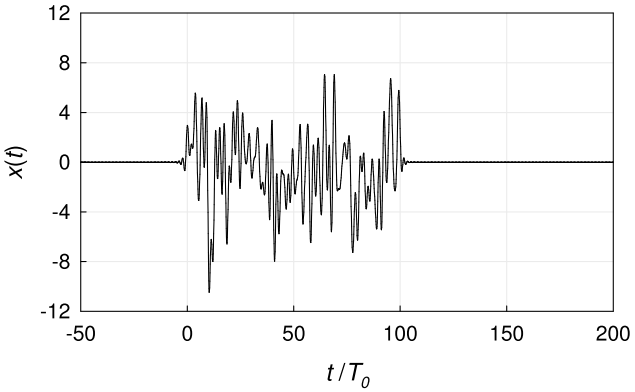

(a) EVD-precoded FTN signaling without power allocation

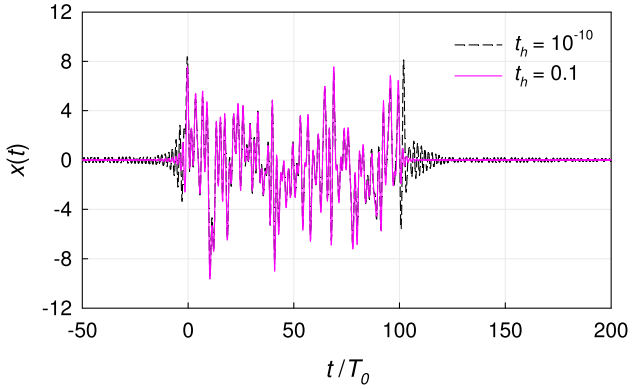

(b) EVD-precoded FTN signaling with truncated power allocation

FIGURE 16. Snapshots of the signal waveforms $x(t)$ of (a) EVD-precoded FTN signaling without power allocation and (b) EVD-precoded FTN signaling with truncated power allocation, where the ISI-free minimum symbol interval was set to $T_0 = 1$ sec. We employed $\tau = 0.1$, $\beta = 0.22$, and $N = 1,000$. Moreover, the threshold for truncated power allocation was set to $t_h = 10^{-10}$ and 0.1.

the ISI-free minimum symbol interval was set to $T_0 = 1$ sec. Hence, the expected total block duration was given by $N\tau T_0 = 100$ sec. For the truncated power allocation scheme, the threshold value was set to $t_h = 10^{-10}$ and 0.1. For the sake of simplicity, BPSK symbols were assigned to the symbols of activated substreams. In Fig. 16(a), most of the transmit energy was within the block interval $[0, N\tau T_0]$, while in Fig. 16(b), the transmit energy was not concentrated within the block interval. More specifically, in EVD-precoded FTN signaling operating without power allocation, the energy outside the block interval was on average only 0.34% of the total transmit energy. Hence, no severe IBI occurs between the adjacent transmitted blocks. However, in EVD-precoded FTN signaling combined with truncated power allocation, on average 10.2% and 1.59% of the total energy was outside the block interval when $t_h = 10^{-10}$ and 0.1, respectively. This energy leakage may cause severe IBI, hence the achievable information rate may be reduced [15]. For $\mathbf{G}^{-\frac{1}{2}}$-precoded FTN signaling, a similar issue associated with the energy outside the block interval was also pointed out in [13]. Note that for practical packing ratio range of $\tau \geq 1/(1+\beta)$, no severe IBI is induced. In [86], in the scenario of EVD-precoded NOFDM combined with power allocation, the impact of inter-frame interference on the achievable information rate was investigated.

IX. ADDITIONAL STUDIES OF FTN SIGNALING

In addition to the aforementioned FTN signaling studies, a variety of other transceiver designs and applications have been investigated [4], [52], which are summarized in Table 11.

A. FTN SIGNALING IN MIMO CHANNEL

While most of the previous FTN signaling studies considered a single-input single-output (SISO) channel, nonetheless FTN signaling in a MIMO channel has also been studied [11], [68], [116], [151]–[155]. In [68], the Mazo limit of a MIMO channel was derived and a space-time block-coded FTN transceiver was developed for a 2×2 MIMO scenario. Most recently, the FTN-MIMO system combined with the space-time multi-mode IM concept was developed in [116], showing that the proposed FTN-MIMO system is capable of achieving better energy efficiency than the Nyquist signaling counterpart.

B. FTN SIGNALING COMBINED WITH NOMA

Moreover, FTN signaling has also been combined with the NOMA concept [43], [117], where the data symbols of each user are transmitted with an FTN-specific symbol interval [117]. In [117], FTN signaling was amalgamated with sparse code multiple access (SCMA) in the uplink, where CE, DD, and user-activity tracking were jointly carried out using a factor-graph-based message passing algorithm. Moreover, the proposed FTN-SCMA scheme was applied to a grant-free transmission scenario. In [43], FTN signaling was exploited in the random-access based NOMA uplink, where similar to [117], iterative joint CE, DD, and user-activity tracking was developed. In [43], [117], it was demonstrated that the bandwidth efficiency is further improved compared to conventional NOMA system by exploiting FTN signaling. Furthermore, similar to the FTN-NOMA system concept, the combination of NOFDM and NOMA was considered in [83].

C. FTN SIGNALING COMBINED WITH IM

As briefly reviewed in Section V-C, FTN-IM signaling, which incorporates the IM concept into FTN signaling, has been studied in [36], [37], [116]. IM is an energy-efficient modulation scheme that implicitly conveys extra information by switching the activation pattern of the TD or FD communication resources, hence it is capable of outperforming classic modulation schemes, such as the PSK and QAM schemes [126], [156]. In [36], IM was combined with FTN signaling for the first time, where the TD SCIM concept was introduced into a FDE-aided FTN system. Owing to exploiting SCIM, higher energy efficiency was achieved than that of conventional FTN signaling operating without IM. In [126], it was shown that FTN-IM signaling achieves a higher constrained information rate than conventional FTN signaling, especially in a low-rate scenario. To further increase the

TABLE 11. Additional studies related to FTN signaling and their contributions.

Year	Authors	Contribution
2012	Zhou [200]	Introduced the concept of generalized FTN signaling with the aid of arbitrary shaping pulses.
2013	Hefnawy and Taoka [201]	Provided an overview of the system model and the capacity of FTN signaling.
	Anderson *et al.* [4]	Provided the first comprehensive survey on FTN signaling studies.
2014	Dasalukunte [202]	Organized the basic theory of FTN signaling and its hardware implementations with the aid of TD detection algorithms.
	Han *et al.* [176]	Formulated a detection problem of binary FTN signaling as a convex optimization problem. Based on the formulated optimization problem, the l_∞-minimization-based symbol recovery method was proposed.
2016	Lucciardi *et al.* [203]	Revealed that when taking into account the effects of an amplifier's non-linearity, FTN signaling with lower-order modulation has the potential to outperform Nyquist signaling with higher-order modulation.
	Kang and Oh [204]	Presented a novel coded FTN system where multiple coded frames were correlated by FTN-induced ISI to construct a long coded frame and increase the coding gain.
	Zhu *et al.* [199]	Applied the FTN signaling concept to an indoor multi-user visible light communication scenario.
	Sasahara *et al.* [177]	Proposed a sum-of-absolute-values optimization detector which is a more efficient convex-optimization-based FTN receiver than that in [176].
2017	Fan *et al.* [52]	Reviewed the previous FTN signaling studies and provided the basic system model of FTN signaling.
	Soltanpur *et al.* [205]	Evaluated the achievable performance of binary FTN signaling in the presence of an unknown jitter at the receiver.
	Landau *et al.* [183]	Exploited the FTN signaling concept to improve the information rate in the scenario of a communication channel using a 1-bit quantized ADC at the receiver.
2018	Zhu *et al.* [206]	Considered a terabit FTN signaling system with the aid of the wavelength-division multiplexing scheme over an optical fiber channel.
	Wang *et al.* [184]	Proposed an FTN-based physical-layer security scheme by exploiting the fact that FTN-induced ISI is unknown at the eavesdropper.
2019	López *et al.* [170]	Proposed a timing synchronization scheme based on the higher-order cyclostationarity of FTN signaling.
2021	Mounsif *et al.* [171]	Developed a pilot-aided timing estimation scheme for FTN signaling, where the optimal pilot sequence was designed for ensuring that the Cramér-Rao lower bound of estimation error is minimized.

energy efficiency, the dual-mode SCIM concept was embedded into FTN signaling in [37]. In [116], the space-time multi-mode IM concept was applied to a GMP-aided FTN-MIMO system. Most recently, in [51], the TD SCIM concept was amalgamated with EVD-precoded FTN signaling combined with optimal power allocation. Furthermore, the IM concept has also been combined with NOFDM [81], [84].

D. OTHER ESTIMATION ISSUES

While the family of CE schemes designed for FTN signaling was reviewed in Section VI-A, a diverse range of other estimation issues such as carrier phase estimation and synchronization designed for FTN signaling were considered in [157]–[165] and [166]–[171], respectively. To elaborate, in [170], a timing synchronization scheme based on exploiting the higher-order cyclostationarity of FTN signaling was proposed. The robustness of this scheme against frequency offsets was characterized in a simple AWGN channel. Furthermore, in [171], a pilot-aided timing estimation scheme was proposed for FTN signaling, where the optimal pilot sequence was designed for ensuring that the Cramér-Rao lower bound of estimation error was minimized.

E. OTHER FTN TRANSCEIVER ARCHITECTURES AND APPLICATIONS

Furthermore, diverse FTN transceiver architectures have been investigated, including a message-passing-based FTN receiver [34], [42], [172]–[175], a convex-optimization-based FTN detector [176], [177], offset-QAM-aided FTN signaling [41], [151], [178]–[181], high-order modulation scheme-assisted FTN signaling [26], [168], [182], and low-resolution analog-to-digital converter (ADC) based FTN signaling [183]. The physical-layer security of FTN signaling was also characterized, for example in [50], [184]. Moreover, FTN signaling has been applied to several specific scenarios other than microwave communications, such as optical communications [47], [130], [137], [139]–[141], [158], [185]–[193], digital video broadcast [160], [194]–[197], the 5G cellular backhaul [198] and visible light communications [199].

X. CONCLUSIONS AND DESIGN GUIDELINES

A. SUMMARY

In this treatise, we reviewed the entire suit of FTN signaling schemes, including low-complexity detection and CE. We then surveyed the information-theoretic framework of unprecoded, filtered and precoded FTN signaling transceiver designs. Furthermore, we presented the theory and fundamental design of the recent EVD-precoded FTN signaling schemes combined with power allocation. We demonstrated that FTN signaling has indeed the potential of achieving a higher capacity than its conventional Nyquist signaling counterpart under the employment of a realistic RRC shaping filter, rather than the ideal rectangular shaping filter.

B. DESIGN GUIDELINE

1) GENERAL TRANSCEIVER STRUCTURES

In general, an FTN transceiver is structured as follows:

- At the transmitter, the information symbols are passed through an RRC shaping filter, having a roll-off factor of β, and are transmitted at an FTN-specific symbol interval of $T = \tau T_0$. The symbol packing ratio and the roll-off factor are set to the range of $0 < \tau \leq 1$ and $0 \leq \beta \leq 1$, respectively.
- At the receiver, the FTN signal is matched-filtered and then sampled at the intervals of $T = \tau T_0$.

- The received samples have to be equalized to eliminate the FTN-induced detrimental ISI effects.

2) PRECODED FTN SIGNALING

The design criteria of precoded FTN signaling are summarized as follows:

- The total energy per block of the precoded FTN signal has to be $N\sigma_s^2$, according to (26).
- In EVD-precoded [15], [16] and ISR-precoded FTN signaling [13], the substreams associated with extremely low eigenvalues may have to be truncated in a low-τ scenario of $\tau < 1/(1+\beta)$. For example, in [15], the threshold was set to $t_h \geq 10^{-10}$ for the scenario of $\beta = 0.22$, $\tau < 0.8$, $N = 10,000$ and standard double-precision numbers. It is practical to set $\tau \geq 1/(1+\beta)$ to avoid the complicated truncation.
- As discussed in Section VII-E, there is a possibility of spectrum broadening when a shaping filter is not strictly bandlimited [129]. Hence, the PSD of precoded FTN signal has to be checked.

C. FUTURE RESEARCH DIRECTIONS

1) FURTHER EFFICIENT CE AND DD

Although a suite of efficient detection algorithms has been conceived for striking compelling performance versus complexity tradeoffs, the associated receiver complexity tends to remain high, especially in a realistic frequency-selective fading scenario. Similarly, further studies of low-complexity iterative CE and DD schemes [35], [39], [42], [43] are required.

2) EXPERIMENTAL CAMPAIGN OF PRECODED FTN SIGNALING

As shown in Section VIII-C, the recent TPC schemes developed for FTN signaling exhibit attractive gains over Nyquist signaling schemes employing a practical RRC shaping filter. However, in the precoded FTN signaling schemes, there is a paucity of experimental campaigns in realistic application scenarios. The potential performance benefits of EVD-precoded FTN signaling combined with power allocation, illustrated in Fig. 15, have to be validated experimentally.

3) BLOCK-BASED FTN TRANSMISSION UNDER THE PRESENCE OF IBI

In most conventional FTN signaling studies, the detrimental IBI effects were typically ignored for the sake of simplicity. Formulating the block-based FTN system model in the presence of IBI and developing its efficient detection algorithm is also an open issue at the time of writing.

GLOSSARY

ADC	Analog-to-Digital Converter
AWGN	Additive White Gaussian Noise
BCJR	Bahl, Cocke, Jelinek, and Raviv
BER	Bit Error Ratio
BPSK	Binary PSK
CDMA	Code-Division Multiple-Access
CE	Channel Estimation
CP	Cyclic Prefix
CSI	Channel State Information
DD	Data Detection
DFE	Decision Feedback Equalization
DFT	Discrete Fourier Transform
DFTN	Differential FTN
EM	Expectation Maximization
EVD	EigenValue Decomposition
EXIT	EXtrinsic Information Transfer
FD	Frequency-Domain
FDE	Frequency-Domain Equalization
FFT	Fast Fourier Transform
FTN	Faster-than-Nyquist
FTNP	FTN-based Pilot
FTN-IM	FTN-index modulation
GMP	Gaussian Message-Passing
HARQ	Hybrid Automatic Repeat Request
IBI	Inter-Block Interference
IDFT	Inverse DFT
IR	Impulse Response
ISI	Inter-Symbol Interference
ISR	Inverse Square Root
LDPC	Low-Density Parity-Check
LPE	Linear Pre-Equalization
MED	Minimum Euclidean Distance
MIMO	Multiple-Input Multiple-Output
MISO	Multiple-Input Single-Output
MLSE	Maximum Likelihood Sequence Estimation
MMSE	Minimum MSE
MSE	Mean Square Error
M-BCJR	M-algorithm based BCJR
NOFDM	Non-Orthogonal Frequency-Division Multiplexing
NOMA	Non-Orthogonal Multiple-Access
OFDM	Orthogonal Frequency-Division Multiplexing
PAM	Pulse-Amplitude Modulation
PR	Partial-Response
PSD	Power Spectral Density
PSK	Phase-Shift Keying
QAM	Quadrature Amplitude Modulation
QPSK	Quadrature PSK
RC	Raised Cosine
RRC	Root RC
RSC	Recursive Systematic Coding
SC-FDMA	Single-Carrier Frequency-Division Multiple Access
SCIM	Single-Carrier Index Modulation
SCMA	sparse code multiple access
SEFDM	Spectrally-Efficient Frequency-Division Multiplexing
SIC	Successive Interference Cancellation

SIMO	Single-Input Multiple-Output
SISO	Single-Input Single-Output
SNR	Signal-to-Noise Ratio
SoD	Soft-Decision
SVD	Singular Value Decomposition
TD	Time-Domain
THP	Tomlinson-Harashima Precoding
TPC	Transmit PreCoding

REFERENCES

[1] D. W. Tufts, "Nyquist's problem—The joint optimization of transmitter and receiver in pulse amplitude modulation," *Proc. IEEE*, vol. 53, no. 3, pp. 248–259, Mar. 1965.
[2] B. Saltzberg, "Intersymbol interference error bounds with application to ideal bandlimited signaling," *IEEE Trans. Inf. Theory*, vol. IT-14, no. 4, pp. 563–568, Jul. 1968.
[3] J. E. Mazo, "Faster-than-Nyquist signaling," *Bell Syst. Tech. J.*, vol. 54, no. 8, pp. 1451–1462, Oct. 1975.
[4] J. B. Anderson, F. Rusek, and V. Öwall, "Faster-than-Nyquist signaling," *Proc. IEEE*, vol. 101, no. 8, pp. 1817–1830, Aug. 2013.
[5] F. Rusek and J. B. Anderson, "Constrained capacities for faster-than-Nyquist signaling," *IEEE Trans. Inf. Theory*, vol. 55, no. 2, pp. 764–775, Feb. 2009.
[6] Y. G. Yoo and J. H. Cho, "Asymptotic optimality of binary faster-than-Nyquist signaling," *IEEE Commun. Lett.*, vol. 14, no. 9, pp. 788–790, Sep. 2010.
[7] A. Modenini, F. Rusek, and G. Colavolpe, "Optimal transmit filters for ISI channels under channel shortening detection," *IEEE Trans. Commun.*, vol. 61, no. 12, pp. 4997–5005, Dec. 2013.
[8] M. E. Hefnawy and G. Kramer, "Impact of spectrum sharing on the efficiency of faster-than-Nyquist signaling," in *Proc. IEEE Wireless Commun. Netw. Conf. (WCNC)*, Apr. 2014, pp. 648–653.
[9] Y. Feng and J. Bajcsy, "Improving throughput of faster-than-Nyquist signaling over multiple-access channels," in *Proc. IEEE 81st Veh. Technol. Conf. (VTC Spring)*, Glasgow, U.K., May 2015, pp. 1–5.
[10] Y. J. D. Kim, J. Bajcsy, and D. Vargas, "Faster-than-Nyquist broadcasting in Gaussian channels: Achievable rate regions and coding," *IEEE Trans. Commun.*, vol. 64, no. 3, pp. 1016–1030, Mar. 2016.
[11] T. E. Bogale, L. B. Le, X. Wang, and L. Vandendorpe, "Multipath multiplexing for capacity enhancement in SIMO wireless systems," *IEEE Trans. Wireless Commun.*, vol. 16, no. 10, pp. 6895–6911, Oct. 2017.
[12] M. Ganji, X. Zou, and H. Jafarkhani, "On the capacity of faster than Nyquist signaling," *IEEE Commun. Lett.*, vol. 24, no. 6, pp. 1197–1201, Jun. 2020.
[13] A. Gattami, E. Ringh, and J. Karlsson, "Time localization and capacity of faster-than-Nyquist signaling," in *Proc. IEEE Global Commun. Conf. (GLOBECOM)*, San Diego, CA, USA, Dec. 2014, pp. 1–7.
[14] Y. J. D. Kim, "Properties of faster-than-Nyquist channel matrices and folded-spectrum, and their applications," in *Proc. IEEE Wireless Commun. Netw. Conf.*, Apr. 2016, pp. 1–7.
[15] T. Ishihara and S. Sugiura, "SVD-precoded faster-than-Nyquist signaling with optimal and truncated power allocation," *IEEE Trans. Wireless Commun.*, vol. 18, no. 12, pp. 5909–5923, Dec. 2019.
[16] K. Masaki, T. Ishihara, and S. Sugiura, "Tradeoff between calculation precision and information rate in eigendecomposition-based faster-than-Nyquist signaling," *IEEE Access*, vol. 8, pp. 223461–223471, 2020.
[17] M. Mohammadkarimi, R. Schober, and V. W. S. Wong, "Channel coding rate for finite blocklength faster-than-Nyquist signaling," *IEEE Commun. Lett.*, vol. 25, no. 1, pp. 64–68, Jan. 2021.
[18] T. Ishihara and S. Sugiura, "Precoded faster-than-Nyquist signaling with optimal power allocation in frequency-selective channel," in *Proc. IEEE Int. Conf. Commun. Workshop*, Jun. 2021, pp. 1–6.
[19] A. D. Liveris and C. N. Georghiades, "Exploiting faster-than-Nyquist signaling," *IEEE Trans. Commun.*, vol. 51, no. 9, pp. 1502–1511, Sep. 2003.
[20] F. Rusek and J. B. Anderson, "Serial and parallel concatenations based on faster than Nyquist signaling," in *Proc. IEEE Int. Symp. Inf. Theory*, Jul. 2006, pp. 1993–1997.
[21] F. Rusek and J. Anderson, "Non binary and precoded faster than Nyquist signaling," *IEEE Trans. Commun.*, vol. 56, no. 5, pp. 808–817, May 2008.
[22] A. Prlja, J. B. Anderson, and F. Rusek, "Receivers for faster-than-Nyquist signaling with and without turbo equalization," in *Proc. IEEE Int. Symp. Inf. Theory*, Jul. 2008, pp. 464–468.
[23] M. McGuire and M. Sima, "Discrete time faster-than-Nyquist signalling," in *Proc. IEEE Global Telecommun. Conf. (GLOBECOM)*, Miami, FL, USA, Dec. 2010, pp. 1–5.
[24] A. Prlja and J. B. Anderson, "Reduced-complexity receivers for strongly narrowband intersymbol interference introduced by faster-than-Nyquist signaling," *IEEE Trans. Commun.*, vol. 60, no. 9, pp. 2591–2601, Sep. 2012.
[25] E. Bedeer, M. H. Ahmed, and H. Yanikomeroglu, "A very low complexity successive symbol-by-symbol sequence estimator for faster-than-Nyquist signaling," *IEEE Access*, vol. 5, pp. 7414–7422, 2017.
[26] E. Bedeer, M. H. Ahmed, and H. Yanikomeroglu, "Low-complexity detection of high-order QAM faster-than-Nyquist signaling," *IEEE Access*, vol. 5, pp. 14579–14588, 2017.
[27] S. Li, B. Bai, J. Zhou, P. Chen, and Z. Yu, "Reduced-complexity equalization for faster-than-Nyquist signaling: New methods based on ungerboeck observation model," *IEEE Trans. Commun.*, vol. 66, no. 3, pp. 1190–1204, Mar. 2018.
[28] X. Wen, W. Yuan, D. Yang, N. Wu, and J. Kuang, "Low complexity message passing receiver for faster-than-Nyquist signaling in nonlinear channels," *IEEE Access*, vol. 6, pp. 68233–68241, 2018.
[29] S. Li, J. Yuan, B. Bai, and N. Benvenuto, "Code-based channel shortening for faster-than-Nyquist signaling: Reduced-complexity detection and code design," *IEEE Trans. Commun.*, vol. 68, no. 7, pp. 3996–4011, Jul. 2020.
[30] S. Sugiura, "Frequency-domain equalization of faster-than-Nyquist signaling," *IEEE Wireless Commun. Lett.*, vol. 2, no. 5, pp. 555–558, Oct. 2013.
[31] S. Sugiura and L. Hanzo, "Frequency-domain-equalization-aided iterative detection of faster-than-Nyquist signaling," *IEEE Trans. Veh. Technol.*, vol. 64, no. 5, pp. 2122–2128, May 2015.
[32] R. Dinis, B. Cunha, F. Ganhao, L. Bernardo, R. Oliveira, and P. Pinto, "A hybrid ARQ scheme for faster than Nyquist signaling with iterative frequency-domain detection," in *Proc. IEEE 81st Veh. Technol. Conf. (VTC Spring)*, May 2015, pp. 1–5.
[33] W. Yuan, N. Wu, H. Wang, and J. Kuang, "Variational inference-based frequency-domain equalization for faster-than-Nyquist signaling in doubly selective channels," *IEEE Signal Process. Lett.*, vol. 23, no. 9, pp. 1270–1274, Sep. 2016.
[34] N. Wu, W. Yuan, H. Wang, Q. Shi, and J. Kuang, "Frequency-domain iterative message passing receiver for faster-than-Nyquist signaling in doubly selective channels," *IEEE Wireless Commun. Lett.*, vol. 5, no. 6, pp. 584–587, Dec. 2016.
[35] T. Ishihara and S. Sugiura, "Iterative frequency-domain joint channel estimation and data detection of faster-than-Nyquist signaling," *IEEE Trans. Wireless Commun.*, vol. 16, no. 9, pp. 6221–6231, Sep. 2017.
[36] T. Ishihara and S. Sugiura, "Faster-than-Nyquist signaling with index modulation," *IEEE Wireless Commun. Lett.*, vol. 6, no. 5, pp. 630–633, Oct. 2017.
[37] M. Nakao, T. Ishihara, and S. Sugiura, "Dual-mode time-domain index modulation for nyquist-criterion and faster-than-Nyquist single-carrier transmissions," *IEEE Access*, vol. 5, pp. 27659–27667, 2017.
[38] T. Ishihara and S. Sugiura, "Differential faster-than-Nyquist signaling," *IEEE Access*, vol. 6, pp. 4199–4206, 2018.
[39] Q. Shi, N. Wu, X. Ma, and H. Wang, "Frequency-domain joint channel estimation and decoding for faster-than-Nyquist signaling," *IEEE Trans. Commun.*, vol. 66, no. 2, pp. 781–795, Feb. 2018.
[40] C. Sagayama, T. Ishihara, and S. Sugiura, "Performance analysis and constellation optimization of star-QAM-aided differential faster-than-Nyquist signaling," *IEEE Signal Process. Lett.*, vol. 26, no. 1, pp. 144–148, Jan. 2019.
[41] T. Hirano, Y. Kakishima, and M. Sawahashi, "TDM based reference signal multiplexing for faster-than-Nyquist signaling using OFDM/OQAM," in *Proc. IEEE Int. Conf. Commun. Syst.*, Macau, China, Nov. 2014, pp. 437–441.
[42] N. Wu, W. Yuan, Q. Guo, and J. Kuang, "A hybrid BP-EP-VMP approach to joint channel estimation and decoding for FTN signaling over frequency selective fading channels," *IEEE Access*, vol. 5, pp. 6849–6858, 2017.
[43] W. Yuan, N. Wu, Q. Guo, D. W. K. Ng, J. Yuan, and L. Hanzo, "Iterative joint channel estimation, user activity tracking, and data detection for FTN-NOMA systems supporting random access," *IEEE Trans. Commun.*, vol. 68, no. 5, pp. 2963–2977, May 2020.

[44] A. Gattami and E. Ringh, "Pre-coding in a faster-than-Nyquist transmission system," U.S. Patent US 9 838 230 B2, Dec. 5, 2017.
[45] B. Qian, X. Wang, J. Wen, S. Zhang, and C. Chen, "Novel intersymbol interference cancellation scheme to enable parallel computational and high-performance faster-than-Nyquist signaling," *IEEE Access*, vol. 5, pp. 24758–24765, 2017.
[46] D. Spano, M. Alodeh, S. Chatzinotas, and B. Ottersten, "Faster-than-Nyquist signaling through spatio-temporal symbol-level precoding for the multiuser MISO downlink channel," *IEEE Trans. Wireless Commun.*, vol. 17, no. 9, pp. 5915–5928, Sep. 2018.
[47] M. Jana, A. Medra, L. Lampe, and J. Mitra, "Pre-equalized faster-than-Nyquist transmission," *IEEE Trans. Commun.*, vol. 65, no. 10, pp. 4406–4418, Oct. 2017.
[48] H. Wang, A. Liu, Z. Feng, X. Liang, H. Liang, and B. Cai, "Iterative-detection-aided Tomlinson-Harashima precoding for faster-than-Nyquist signaling," *IEEE Access*, vol. 8, pp. 7748–7757, 2020.
[49] Y. Li, S. Xiao, J. Wang, and W. Tang, "Cholesky-decomposition aided linear precoding and decoding for FTN signaling," *IEEE Wireless Commun. Lett.*, vol. 10, no. 6, pp. 1163–1167, Jun. 2021.
[50] S. Sugiura, "Secrecy performance of eigendecomposition-based FTN signaling and NOFDM in quasi-static fading channel," *IEEE Trans. Wireless Commun.*, early access, Apr. 12, 2021, doi: 10.1109/TWC.2021.3070891.
[51] P. Chaki, T. Ishihara, and S. Sugiura, "Eigenvalue decomposition precoded faster-than-Nyquist transmission of index modulated symbols," in *Proc. IEEE Int. Symp. Inf. Theory (ISIT)*, Jul. 2021, pp. 1–6.
[52] J. Fan, S. Guo, X. Zhou, Y. Ren, G. Y. Li, and X. Chen, "Faster-than-Nyquist signaling: An overview," *IEEE Access*, vol. 5, pp. 1925–1940, 2017.
[53] L. Hanzo, T. Liew, B. Yeap, R. Y. S. Tee, and S. X. Ng, *Turbo Coding, Turbo Equalisation, and Space-Time Coding for Transmission Over Fading Channels*. Hoboken, NJ, USA: Wiley, 2011.
[54] S. Sugiura, S. Chen, and L. Hanzo, "MIMO-aided near-capacity turbo transceivers: Taxonomy and performance versus complexity," *IEEE Commun. Surveys Tuts.*, vol. 14, no. 2, pp. 421–442, 2nd Quart., 2012.
[55] J. G. Proakis and M. Salehi, *Digital Communications*. New York, NY, USA: McGraw-Hill, 1995.
[56] A. Goldsmith, *Wireless Communications*. Cambridge, U.K.: Cambridge Univ. Press, 2005.
[57] J. B. Anderson and A. Svensson, *Coded Modulation Systems*. New York, NY, USA: Kluwer/Plenum, 2003.
[58] R. W. Lucky, "Decision feedback and faster-than-Nyquist transmission," in *Proc. IEEE Int. Symp. Inf. Theory*, Noordwijk, The Netherlands, Jun. 1970, pp. 15–19.
[59] J. Salz, "Optimum mean-square decision feedback equalization," *Bell Syst. Tech. J.*, vol. 52, no. 8, pp. 1341–1373, Oct. 1973.
[60] G. J. Foschini, "Contrasting performance of faster binary signaling with QAM," *AT&T Bell Laboratories Tech. J.*, vol. 63, no. 8, pp. 1419–1445, Oct. 1984.
[61] A. Fihel and H. Sari, "Performance of reduced-bandwidth 16 QAM with decision-feedback equalization," *IEEE Trans. Commun.*, vol. COM-35, no. 7, pp. 715–723, Jul. 1987.
[62] C.-K. Wang and L.-S. Lee, "Practically realizable digital transmission significantly below the Nyquist bandwidth," *IEEE Trans. Commun.*, vol. 43, nos. 2–4, pp. 166–169, Feb. 1995.
[63] D. Hajela, "Some new results on faster than Nyquist signaling," in *Proc. Conf. Inf. Sci. Syst.* Baltimore, MD, USA: Johns Hopkins Univ., Mar. 1987, pp. 399–403.
[64] D. Hajela, "On computing the minimum distance for faster than Nyquist signaling," in *Proc. Conf. Inf. Sci. Syst.* Baltimore, MD, USA: Johns Hopkins Univ., Mar. 1987, pp. 399–403.
[65] J. E. Mazo and H. J. Landau, "On the minimum distance problem for faster-than-Nyquist signaling," *IEEE Trans. Inf. Theory*, vol. IT-34, no. 6, pp. 1420–1427, Nov. 1988.
[66] D. Hajela, "On faster than nyquist signaling: Computing the minimum distance," *J. Approximation Theory*, vol. 63, no. 1, pp. 108–120, Oct. 1990.
[67] D. Hajela, "On computing the minimum distance for faster than nyquist signaling," *IEEE Trans. Inf. Theory*, vol. 36, no. 2, pp. 289–295, Mar. 1990.
[68] F. Rusek, "On the existence of the mazo-limit on MIMO channels," *IEEE Trans. Wireless Commun.*, vol. 8, no. 3, pp. 1118–1121, Mar. 2009.
[69] M. Rodrigues and I. Darwazeh, "A spectrally efficient frequency division multiplexing based communications system," in *Proc. 8th Int. OFDM Workshop*, 2003, pp. 48–49.
[70] I. Kanaras, A. Chorti, M. R. D. Rodrigues, and I. Darwazeh, "Spectrally efficient FDM signals: Bandwidth gain at the expense of receiver complexity," in *Proc. IEEE Int. Conf. Commun.*, Dresden, Germany, Jun. 2009, pp. 1–6.
[71] S. Isam and I. Darwazeh, "Precoded spectrally efficient FDM system," in *Proc. 21st Annu. IEEE Int. Symp. Pers., Indoor Mobile Radio Commun.*, Istanbul, Turkey, Sep. 2010, pp. 99–104.
[72] S. Isam, I. Kanaras, and I. Darwazeh, "A truncated SVD approach for fixed complexity spectrally efficient FDM receivers," in *Proc. IEEE Wireless Commun. Netw. Conf.*, Cancun, Mexico, Mar. 2011, pp. 1584–1589.
[73] P. N. Whatmough, M. R. Perrett, S. Isam, and I. Darwazeh, "VLSI architecture for a reconfigurable spectrally efficient FDM baseband transmitter," *IEEE Trans. Circuits Syst. I, Reg. Papers*, vol. 59, no. 5, pp. 1107–1118, May 2012.
[74] S. Isam and I. Darwazeh, "Robust channel estimation for spectrally efficient FDM system," in *Proc. 19th Int. Conf. Telecommun. (ICT)*, Jounieh, Lebanon, Apr. 2012, pp. 1–6.
[75] I. Darwazeh, T. Xu, T. Gui, Y. Bao, and Z. Li, "Optical SEFDM system; bandwidth saving using non-orthogonal sub-carriers," *IEEE Photon. Technol. Lett.*, vol. 26, no. 4, pp. 352–355, Feb. 2014.
[76] T. Xu and I. Darwazeh, "A soft detector for spectrally efficient systems with non-orthogonal overlapped sub-carriers," *IEEE Commun. Lett.*, vol. 18, no. 10, pp. 1847–1850, Oct. 2014.
[77] D. Rainnie, Y. Feng, and J. Bajcsy, "On capacity merits of spectrally efficient FDM," in *Proc. IEEE Mil. Commun. Conf. (MILCOM)*, Tampa, FL, USA, Oct. 2015, pp. 581–586.
[78] S. V. Zavjalov, S. V. Volvenko, and S. B. Makarov, "A method for increasing the spectral and energy efficiency SEFDM signals," *IEEE Commun. Lett.*, vol. 20, no. 12, pp. 2382–2385, Dec. 2016.
[79] I. Darwazeh, H. Ghannam, and T. Xu, "The first 15 years of SEFDM: A brief survey," in *Proc. 11th Int. Symp. Commun. Syst., Netw. Digit. Signal Process. (CSNDSP)*, Budapest, Hungary, Jul. 2018, pp. 1–7.
[80] Y. Feng, Y. Ma, Z. Li, C. Yan, and N. Wu, "Low-complexity factor graph-based iterative detection for RRC-SEFDM signals," in *Proc. 10th Int. Conf. Wireless Commun. Signal Process. (WCSP)*, Hangzhou, China, Oct. 2018, pp. 1–6.
[81] M. Nakao and S. Sugiura, "Spectrally efficient frequency division multiplexing with index-modulated non-orthogonal subcarriers," *IEEE Wireless Commun. Lett.*, vol. 8, no. 1, pp. 233–236, Feb. 2019.
[82] S. Osaki, M. Nakao, T. Ishihara, and S. Sugiura, "Differentially modulated spectrally efficient frequency-division multiplexing," *IEEE Signal Process. Lett.*, vol. 26, no. 7, pp. 1046–1050, Jul. 2019.
[83] D. Li, M. Jia, X. Wang, Q. Guo, and X. Gu, "Iterative multiuser detection and decoding for sparse code multiple access combined with spectrally efficient frequency division multiplexing," *IEEE Access*, vol. 8, pp. 24887–24895, 2020.
[84] Y. Ma, N. Wu, W. Yuan, D. W. K. Ng, and L. Hanzo, "Joint channel estimation and equalization for index-modulated spectrally efficient frequency division multiplexing systems," *IEEE Trans. Commun.*, vol. 68, no. 10, pp. 6230–6244, Oct. 2020.
[85] S. Osaki, T. Ishihara, and S. Sugiura, "Eigenvalue-decomposition-precoded ultra-dense non-orthogonal frequency-division multiplexing," *IEEE Trans. Wireless Commun.*, vol. 19, no. 12, pp. 8165–8178, Dec. 2020.
[86] S. Osaki and S. Sugiura, "Impact of inter-frame interference on eigendecomposition-precoded non-orthogonal frequency-division multiplexing," *IEEE Wireless Commun. Lett.*, early access, Apr. 20, 2021, doi: 10.1109/LWC.2021.3074504.
[87] F. Rusek and J. B. Anderson, "The two dimensional mazo limit," in *Proc. Int. Symp. Inf. Theory (ISIT)*, Adelaide, SA, Australia, Sep. 2005, pp. 970–974.
[88] J. B. Anderson and F. Rusek, "Improving OFDM: Multistream faster-than-Nyquist signaling," in *Proc. 6th Int. ITG-Conf. Source Channel Coding*, Munich, Germany, Apr. 2006, pp. 1–5.
[89] F. Rusek and J. B. Anderson, "Successive interference cancellation in multistream faster-than-Nyquist signaling," in *Proc. Int. Conf. Commun. mobile Comput. (IWCMC)*. New York, NY, USA: ACM, 2006, pp. 1021–1026.
[90] F. Rusek and J. B. Anderson, "Multistream faster than nyquist signaling," *IEEE Trans. Commun.*, vol. 57, no. 5, pp. 1329–1340, May 2009.
[91] A. Barbieri, D. Fertonani, and G. Colavolpe, "Time-frequency packing for linear modulations: Spectral efficiency and practical detection schemes," *IEEE Trans. Commun.*, vol. 57, no. 10, pp. 2951–2959, Oct. 2009.

[92] D. Dasalukunte, F. Rusek, and V. Owall, "An iterative decoder for multicarrier faster-than-Nyquist signaling systems," in *Proc. IEEE Int. Conf. Commun.*, Cape Town, South Africa, May 2010, pp. 1–5.
[93] D. Dasalukunte, F. Rusek, and V. Owall, "Multicarrier faster-than-Nyquist transceivers: Hardware architecture and performance analysis," *IEEE Trans. Circuits Syst. I, Reg. Papers*, vol. 58, no. 4, pp. 827–838, Apr. 2011.
[94] D. Dasalukunte, F. Rusek, and V. Owall, "An 0.8-mm^2 9.6-mW iterative decoder for faster-than-Nyquist and orthogonal signaling multicarrier systems in 65-nm CMOS," *IEEE J. Solid-State Circuits*, vol. 48, no. 7, pp. 1680–1688, Jul. 2013.
[95] F. Schaich and T. Wild, "A reduced complexity receiver for multi-carrier faster-than-Nyquist signaling," in *Proc. IEEE Globecom Workshops (GC Wkshps)*, Atlanta, GA, USA, Dec. 2013, pp. 235–240.
[96] M. Secondini, T. Foggi, F. Fresi, G. Meloni, F. Cavaliere, G. Colavolpe, E. Forestieri, L. Píti, R. Sabella, and G. Prati, "Optical time–frequency packing: Principles, design, implementation, and experimental demonstration," *J. Lightw. Technol.*, vol. 33, no. 17, pp. 3558–3570, Sep. 1, 2015.
[97] S. Peng, A. Liu, H. Fang, K. Wang, and X. Liang, "Turbo frequency domain equalization and detection for multicarrier faster-than-Nyquist signaling," in *Proc. IEEE Wireless Commun. Netw. Conf. (WCNC)*, San Francisco, CA, USA, Mar. 2017, pp. 1–6.
[98] S. Peng, A. Liu, X. Pan, and H. Wang, "Hexagonal multicarrier faster-than-Nyquist signaling," *IEEE Access*, vol. 5, pp. 3332–3339, 2017.
[99] S. Peng, A. Liu, X. Tong, and K. Wang, "On max-SIR time–frequency packing for multicarrier faster-than-Nyquist signaling," *IEEE Commun. Lett.*, vol. 21, no. 10, pp. 2142–2145, Oct. 2017.
[100] S. Peng, A. Liu, K. Wang, and X. Liang, "PAPR reduction of multicarrier faster-than-Nyquist signals with partial transmit sequence," *IEEE Access*, vol. 5, pp. 24931–24937, 2017.
[101] A. Liu, S. Peng, L. Song, X. Liang, K. Wang, and Q. Zhang, "Peak-to-Average power ratio of multicarrier faster-than-Nyquist signals: Distribution, optimization and reduction," *IEEE Access*, vol. 6, pp. 11977–11987, 2018.
[102] S. Peng, A. Liu, L. Song, I. Memon, and H. Wang, "Spectral efficiency maximization for deliberate clipping-based multicarrier faster-than-Nyquist signaling," *IEEE Access*, vol. 6, pp. 13617–13623, 2018.
[103] S. Peng, A. Liu, X. Tong, and G. Colavolpe, "An efficient implementation of lattice staggered multicarrier faster-than-Nyquist signaling," *IEEE Commun. Lett.*, vol. 22, no. 2, pp. 240–243, Feb. 2018.
[104] S. Peng, A. Liu, X. Liu, K. Wang, and X. Liang, "MMSE turbo equalization and detection for multicarrier faster-than-Nyquist signaling," *IEEE Trans. Veh. Technol.*, vol. 67, no. 3, pp. 2267–2275, Mar. 2018.
[105] F. Tian, Y. Feng, Y. Ma, and N. Wu, "Gaussian message passing based receiver for multicarrier faster-than-Nyquist signaling," in *Proc. 10th Int. Conf. Wireless Commun. Signal Process. (WCSP)*, Hangzhou, China, Oct. 2018, pp. 1–6.
[106] K. Wang, A. Liu, X. Liang, S. Peng, and Q. Zhang, "A faster-than-Nyquist (FTN)-based multicarrier system," *IEEE Trans. Veh. Technol.*, vol. 68, no. 1, pp. 947–951, Jan. 2019.
[107] M. Jana, L. Lampe, and J. Mitra, "Precoded time-frequency-packed multicarrier faster-than-Nyquist transmission," in *Proc. IEEE 20th Int. Workshop Signal Process. Adv. Wireless Commun. (SPAWC)*, Cannes, France, Jul. 2019, pp. 1–5.
[108] B. Cai, A. Liu, and X. Liang, "Low-complexity partial transmit sequence methods using dominant time-domain samples for multicarrier faster-than-Nyquist signaling," *IEEE Access*, vol. 7, pp. 121552–121564, 2019.
[109] Y. Ma, F. Tian, N. Wu, B. Li, and X. Ma, "A low-complexity receiver for multicarrier faster-than-Nyquist signaling over frequency selective channels," *IEEE Commun. Lett.*, vol. 24, no. 1, pp. 81–85, Jan. 2020.
[110] B. Cai, A. Liu, and X. Liang, "Low-complexity selective mapping methods for multicarrier faster-than-Nyquist signaling," *IEEE Access*, vol. 8, pp. 31420–31431, 2020.
[111] Y. J. D. Kim and Y. Feng, "Capacity of multicarrier faster-than-Nyquist signaling," in *Proc. IEEE Int. Symp. Inf. Theory (ISIT)*, Los Angeles, CA, USA, Jun. 2020, pp. 2049–2054.
[112] H. Che, K. Zhu, and Y. Bai, "Multicarrier faster-than-Nyquist based on efficient implementation and probabilistic shaping," *IEEE Access*, vol. 9, pp. 63943–63951, 2021.
[113] T. Strohmer and S. Beaver, "Optimal OFDM design for time-frequency dispersive channels," *IEEE Trans. Commun.*, vol. 51, no. 7, pp. 1111–1122, Jul. 2003.
[114] M.-S. Baek, N.-H. Hur, and H. Lim, "Novel interference cancellation technique based on matrix computation for FTN communication system," in *Proc. IEEE Mil. Commun. Conf.*, Baltimore, MD, USA, Oct. 2014, pp. 830–834.
[115] J. Fan, Y. Ren, Y. Zhang, and X. Luo, "MLSE equalizer with channel shortening for faster-than-Nyquist signaling," *IEEE Photon. Technol. Lett.*, vol. 30, no. 9, pp. 793–796, May 1, 2018.
[116] S. Li, N. Wu, Q. Shi, and Q. Guo, "FTN signaling-aided space-time multi-mode index modulation systems with a GMP-based receiver," *IEEE Access*, vol. 7, pp. 162898–162912, 2019.
[117] W. Yuan, N. Wu, A. Zhang, X. Huang, Y. Li, and L. Hanzo, "Iterative receiver design for FTN signaling aided sparse code multiple access," *IEEE Trans. Wireless Commun.*, vol. 19, no. 2, pp. 915–928, Feb. 2020.
[118] J. B. Anderson, A. Prlja, and F. Rusek, "New reduced state space BCJR algorithms for the ISI channel," in *Proc. IEEE Int. Symp. Inf. Theory*, Jun. 2009, pp. 889–893.
[119] J. B. Anderson and A. Prlja, "Turbo equalization and an M-BCJR algorithm for strongly narrowband intersymbol interference," in *Proc. Int. Symp. Inf. Theory Appl.*, Oct. 2010, pp. 261–266.
[120] S. Nie, M. Guo, and Y. Shen, "Interference cancellation technique for faster-than-Nyquist signalling," *Electron. Lett.*, vol. 52, no. 13, pp. 1126–1128, Jun. 2016.
[121] H. Fukumoto and K. Hayashi, "Overlap frequency domain equalization for faster-than-Nyquist signaling," 2015, *arXiv:1509.00562*. [Online]. Available: http://arxiv.org/abs/1509.00562
[122] N. Al-Dhahir, "Single-carrier frequency-domain equalization for space-time block-coded transmissions over frequency-selective fading channels," *IEEE Commun. Lett.*, vol. 5, no. 7, pp. 304–306, Jul. 2001.
[123] D. Falconer, S. L. Ariyavisitakul, A. Benyamin-Seeyar, and B. Eidson, "Frequency domain equalization for single-carrier broadband wireless systems," *IEEE Commun. Mag.*, vol. 40, no. 4, pp. 58–66, Apr. 2002.
[124] S. Li, W. Yuan, J. Yuan, B. Bai, D. Wing Kwan Ng, and L. Hanzo, "Time-domain vs. frequency-domain equalization for FTN signaling," *IEEE Trans. Veh. Technol.*, vol. 69, no. 8, pp. 9174–9179, Aug. 2020.
[125] M. Nakao, T. Ishihara, and S. Sugiura, "Single-carrier frequency-domain equalization with index modulation," *IEEE Commun. Lett.*, vol. 21, no. 2, pp. 298–301, Feb. 2017.
[126] S. Sugiura, T. Ishihara, and M. Nakao, "State-of-the-art design of index modulation in the space, time, and frequency domains: Benefits and fundamental limitations," *IEEE Access*, vol. 5, pp. 21774–21790, 2017.
[127] S. Gao, L. Lin, Y. Lin, H. Zhang, and D. Pan, "Pilot design for channel estimation in a long-tap faster-than-Nyquist signaling transmission," in *Proc. IEEE 17th Int. Conf. Commun. Technol. (ICCT)*, Chengdu, China, Oct. 2017, pp. 261–265.
[128] B. Cai, A. Liu, X. Tong, and F. Cheng, "Training sequences design for channel estimation in FTN system using discrete Fourier transform techniques," *IET Commun.*, vol. 11, no. 17, pp. 2561–2565, Nov. 2017.
[129] Y. J. D. Kim and J. Bajcsy, "On spectrum broadening of pre-coded faster-than-Nyquist signaling," in *IEEE 72nd Veh. Technol. Conf. (VTC)*, Ottawa, ON, Canada, Sep. 2010, pp. 1–5.
[130] M. Jana, L. Lampe, and J. Mitra, "Dual-polarized faster-than-Nyquist transmission using higher order modulation schemes," *IEEE Trans. Commun.*, vol. 66, no. 11, pp. 5332–5345, Nov. 2018.
[131] H. Che, Z. Wu, and W. Kang, "Inner code optimization for high rate faster-than-Nyquist," in *Proc. IEEE Wireless Commun. Netw. Conf. (WCNC)*, Marrakesh, Morocco, Apr. 2019.
[132] S. Wen, G. Liu, Q. Chen, H. Qu, Y. Wang, and P. Zhou, "Optimization of precoded FTN signaling with MMSE-based turbo equalization," in *Proc. IEEE Int. Conf. Commun. (ICC)*, Shanghai, China, May 2019, pp. 1–6.
[133] S. An, J. Li, X. Li, and Y. Su, "FTN SSB 16-QAM signal transmission and direct detection based on tomlinson-harashima precoding with computed coefficients," *J. Lightw. Technol.*, vol. 39, no. 7, pp. 2059–2066, Apr. 1, 2021.
[134] H. Wang, A. Liu, X. Liang, S. Peng, and K. Wang, "Linear precoding for faster-than-Nyquist signaling," in *Proc. 3rd IEEE Int. Conf. Comput. Commun. (ICCC)*, Chengdu, China, Dec. 2017, pp. 52–56.
[135] A. Modenini, F. Rusek, and G. Colavolpe, "Faster-than-Nyquist signaling for next generation communication architectures," in *Proc. 22nd Eur. Signal Process. Conf. (EUSIPCO)*, Lisbon, Portugal, Sep. 2014, pp. 1856–1860.
[136] M. Yuhas, Y. Feng, and J. Bajcsy, "On the capacity of faster-than-Nyquist MIMO transmission with CSI at the receiver," in *Proc. IEEE Globecom Workshops*, San Diego, CA, USA, Dec. 2015, pp. 1–6.
[137] D. Chang, O. Omomukuyo, O. Dobre, R. Venkatesan, and P. Gillard, "A faster-than-Nyquist PDM-16QAM scheme enabled by tomlinson-harashima precoding," in *Proc. 17th Int. Conf. Transparent Opt. Netw. (ICTON)*, Budapest, Hungary, Jul. 2015, pp. 1–4.
[138] D. Chang, O. Omomukuyo, O. Dobre, R. Venkatesan, P. Gillard, and C. Rumbolt, "Tomlinson-harashima precoding with soft detection for faster than nyquist DP-16QAM coherent optical systems," in *Proc. Opt. Fiber Commun. Conf.*, Los Angeles, CA, USA, Mar. 2015, pp. 1–3.

[139] D. Chang, O. Omomukuyo, X. Lin, S. Zhang, O. A. Dobre, and R. Venkatesan, "Robust faster-than-Nyquist PDM-mQAM systems with Tomlinson–Harashima precoding," *IEEE Photon. Technol. Lett.*, vol. 28, no. 19, pp. 2106–2109, Oct. 1, 2016.
[140] N. Kikuchi, R. Hirai, and T. Fukui, "Application of Tomlinson-Harashima precoding (THP) for short-reach band-limited nyquist PAM and faster-than-Nyquist PAM signaling," in *Proc. Opt. Fiber Commun. Conf. Expo.*, Mar. 2018, pp. 1–3.
[141] Q. Hu, K. Schuh, M. Chagnon, F. Buchali, and H. Bulow, "Up to 94 GBd THP PAM-4 transmission with 33 GHz bandwidth limitation," in *Proc. Eur. Conf. Opt. Commun. (ECOC)*, Rome, Italy, Sep. 2018, pp. 1–3.
[142] C. E. Shannon, "A mathematical theory of communication," *Bell Syst. Tech. J.*, vol. 27, no. 3, pp. 379–423, Jul. 1948.
[143] Y. J. D. Kim and J. Bajcsy, "Information rates of cyclostationary faster-than-Nyquist signaling," in *Proc. 12th Can. Workshop Inf. Theory*, May 2011, pp. 1–4.
[144] M. E. Hefnawy, G. Dietl, and G. Kramer, "Spectral shaping for faster-than-Nyquist signaling," in *Proc. 11th Int. Symp. Wireless Commun. Syst. (ISWCS)*, Barcelona, Spain, Aug. 2014, pp. 496–500.
[145] F. Rusek, "A first encounter with faster-than-Nyquist signaling on the MIMO channel," in *Proc. IEEE Wireless Commun. Netw. Conf.*, Kowloon, China, Mar. 2007, pp. 1093–1097.
[146] Y. J. D. Kim, "Faster than Nyquist transmission over continuous-time channels: Capacity analysis and coding," Ph.D. dissertation, Dept. Elect. Comput. Eng., McGill Univ., Montreal, QC, Canada, 2013.
[147] Y. Polyanskiy, H. V. Poor, and S. Verdu, "Channel coding rate in the finite blocklength regime," *IEEE Trans. Inf. Theory*, vol. 56, no. 5, pp. 2307–2359, May 2010.
[148] J. M. Varah, "The prolate matrix," *Linear Algebra its Appl.*, vol. 187, pp. 269–278, Jul. 1993.
[149] T. Strohmer, "Numerical analysis of the non-uniform sampling problem," *J. Comput. Appl. Math.*, vol. 122, nos. 1–2, pp. 297–316, Oct. 2000.
[150] A. SaiToh, "ZKCM: A C++ library for multiprecision matrix computation with applications in quantum information," *Comput. Phys. Commun.*, vol. 184, no. 8, pp. 2005–2020, Aug. 2013.
[151] K. Yagishita, Y. Kakishima, and M. Sawahashi, "Effects of antenna receiver diversity with faster-than-Nyquist signaling using OFDM/OQAM in multipath fading channel," in *Proc. Int. Symp. Wireless Pers. Multimedia Commun. (WPMC)*, Sydney, NSW, Australia, Sep. 2014, pp. 351–355.
[152] B. G. Jo, M. C. Park, and D. S. Han, "SM-MIMO scheme with FTN signalling for UHDTV," in *Proc. IEEE Int. Conf. Consum. Electron. (ICCE)*, Las Vegas, NV, USA, Jan. 2016, pp. 514–515.
[153] G.-W. Park and J.-W. Jung, "A study on MIMO-FTN scheme based on layered space time code using turbo codes," in *Proc. 8th Int. Conf. Ubiquitous Future Netw. (ICUFN)*, Vienna, Austria, Jul. 2016, pp. 505–507.
[154] A. T. Abebe and C. G. Kang, "FTN-based MIMO transmission as a NOMA scheme for efficient coexistence of broadband and sporadic traffics," in *Proc. IEEE 87th Veh. Technol. Conf. (VTC Spring)*, Porto, Portugal, Jun. 2018, pp. 1–5.
[155] B. Lee, J. Kim, H. Lee, B. Shim, Y. Kim, and J. Lee, "Towards faster-than-Nyquist transmission for beyond 5G wireless communications," in *Proc. IEEE Int. Conf. Commun. (ICC)*, Shanghai, China, May 2019, pp. 1–6.
[156] N. Ishikawa, S. Sugiura, and L. Hanzo, "Subcarrier-index modulation aided OFDM—Will it work?" *IEEE Access*, vol. 4, pp. 2580–2593, 2016.
[157] X. Liang, A. Liu, X. Pan, and F. Chen, "Method for carrier frequency-offset estimation of faster-than-Nyquist signalling," *Electron. Lett.*, vol. 51, no. 25, pp. 2151–2153, Dec. 2015.
[158] X. Zhang, D. Pan, and Y. Feng, "A new carrier phase recovery method in faster than nyquist optical fiber communication system," in *Proc. 14th Int. Conf. Opt. Commun. Netw. (ICOCN)*, Nanjing, China, Jul. 2015, pp. 1–3.
[159] D. Pan, C. Li, Y. Feng, and X. Zhang, "An effective carrier phase estimation scheme in faster than nyquist WDM transmission system," *Photonic Netw. Commun.*, vol. 32, no. 2, pp. 253–258, Feb. 2016, doi: 10.1007/s11107-015-0595-y.
[160] H.-J. Kim and J.-S. Seo, "Carrier frequency offset estimation for faster-than nyquist transmission in DVB-S2 systems," in *Proc. IEEE Int. Symp. Broadband Multimedia Syst. Broadcast. (BMSB)*, Nara, Japan, Jun. 2016, pp. 1–4.
[161] X. Liang, A. Liu, H. Wang, K. Wang, and S. Peng, "Method of NDA frequency-offset estimation for faster-than-Nyquist signaling with high-order modulation," in *Proc. IEEE/CIC Int. Conf. Commun. China (ICCC)*, Chengdu, China, Jul. 2016, pp. 1–4.
[162] C. Li, D. Pan, Y. Feng, and X. Zhang, "A modified viterbi and viterbi phase estimation scheme in faster than nyquist optical communication system," in *Proc. 15th Int. Conf. Opt. Commun. Netw. (ICOCN)*, Hangzhou, China, Sep. 2016, pp. 1–3.
[163] X. Qi, N. Wu, L. Zhou, D. Yang, and H. Wang, "Joint phase noise estimation and iterative detection of faster-than-Nyquist signaling based on factor graph," in *Proc. IEEE 85th Veh. Technol. Conf. (VTC Spring)*, Sydney, NSW, Australia, Jun. 2017.
[164] P. Cheng, A. Liu, X. Liang, K. Wang, and B. Cai, "The estimation and tracking for frequency offset in faster-than-Nyquist signaling," in *Proc. 3rd IEEE Int. Conf. Comput. Commun. (ICCC)*, Chengdu, China, Dec. 2017, pp. 1353–1357.
[165] J. Fan, Y. Ren, Y. Zhang, and X. Luo, "Iterative carrier frequency offset estimation for faster-than-Nyquist signaling," in *Proc. 20th Int. Symp. Wireless Pers. Multimedia Commun. (WPMC)*, Bali, Indonesia, Dec. 2017, pp. 150–153.
[166] P. Kim and D.-G. Oh, "Synchronization for faster than nyquist signalling transmission," in *Proc. 7th Int. Conf. Ubiquitous Future Netw.*, Sapporo, Japan, Jul. 2015, pp. 944–949.
[167] M. C. Park, B. G. Jo, Y. Kim, H. Lim, and D. S. Han, "Synchronization of FTN systems for UHDTV," in *Proc. IEEE Int. Conf. Consum. Electron. (ICCE)*, Las Vegas, NV, USA, Jan. 2016, pp. 417–418.
[168] X. Liang, A. Liu, B. Gao, and K. Wang, "Method of timing estimation for FTN signalling with high-order modulation," *Electron. Lett.*, vol. 52, no. 13, pp. 1134–1136, Jun. 2016.
[169] J.-A. Lucciardi, N. Thomas, M.-L. Boucheret, C. Poulliat, and G. Mesnager, "Receiver for FTN signaling in non-linear channel: Joint channel estimation and synchronization," in *Proc. IEEE 28th Annu. Int. Symp. Pers., Indoor, Mobile Radio Commun. (PIMRC)*, Montreal, QC, Canada, Oct. 2017, pp. 1–7.
[170] M. J. L. Morales, D. Roque, and M. Benammar, "Timing estimation based on higher order cyclostationarity for faster-than-Nyquist signals," *IEEE Commun. Lett.*, vol. 23, no. 8, pp. 1373–1376, Aug. 2019.
[171] L. Mounsif and D. Roque, "Optimal pilot sequences for timing estimation in faster-than-Nyquist systems," *IEEE Commun. Lett.*, vol. 25, no. 4, pp. 1236–1240, Apr. 2021.
[172] P. Sen, T. Aktas, and A. O. Yilmaz, "A low-complexity graph-based LMMSE receiver designed for colored noise induced by FTN-signaling," in *Proc. IEEE Wireless Commun. Netw. Conf. (WCNC)*, Istanbul, Turkey, Apr. 2014, pp. 642–647.
[173] K. Kihara, T. Nishimura, T. Ohgane, and Y. Ogawa, "Signal detection with belief propagation in faster-than-Nyquist signaling," in *Proc. Asia–Pacific Signal Inf. Process. Assoc. Annu. Summit Conf. (APSIPA ASC)*, Kuala Lumpur, Malaysia, Dec. 2017, pp. 1790–1794.
[174] T. Yu, M. Zhao, J. Zhong, and Y. Cai, "Low-complexity detection for FTN signaling based on weighted FG-SS-BP equalization method," in *Proc. IEEE 83rd Veh. Technol. Conf. (VTC Spring)*, Nanjing, China, May 2016, pp. 1–5.
[175] T. Yu, M. Zhao, J. Zhong, J. Zhang, and P. Xiao, "Low-complexity graph-based turbo equalisation for single-carrier and multi-carrier FTN signalling," *IET Signal Process.*, vol. 11, no. 7, pp. 838–845, Sep. 2017.
[176] F. Han, M. Jin, and H. Zou, "Binary symbol recovery via ℓ_∞ minimization in faster-than-Nyquist signaling systems," *IEEE Trans. Signal Process.*, vol. 62, no. 20, pp. 5282–5293, Oct. 2014.
[177] H. Sasahara, K. Hayashi, and M. Nagahara, "Symbol detection for faster-than-Nyquist signaling by sum-of-absolute-values optimization," *IEEE Signal Process. Lett.*, vol. 23, no. 12, pp. 1853–1857, Dec. 2016.
[178] H. Lin, N. Lahbabi, P. Siohan, and X. Jiang, "An efficient FTN implementation of the OFDM/OQAM system," in *Proc. IEEE Int. Conf. Commun. (ICC)*, London, U.K., Jun. 2015, pp. 4787–4792.
[179] Y. Yamada, M. Sawahashi, and K. Saito, "Faster-than-Nyquist signaling with non-uniform compression factors for OFDM/OQAM," in *Proc. Int. Symp. Intell. Signal Process. Commun. Syst. (ISPACS)*, Nov. 2015, pp. 520–525.
[180] N. Lahbabi, H. Lin, C. A. Nour, C. Douillard, and P. Siohan, "Sparse interference pre-cancellation for FTN-OQAM systems," in *Proc. Eur. Wireless Conf.*, Oulu, Finland, May 2016, pp. 1–6.
[181] N. Lahbabi, H. Lin, C. A. Nour, C. Douillard, and P. Siohan, "An enhanced coding strategy for FTN-OFDM/OQAM transceiver design," in *Proc. IEEE Int. Conf. Commun. (ICC)*, Paris, France, May 2017, pp. 1–6.
[182] J. Yu, J. Park, F. Rusek, B. Kudryashov, and I. Bocharova, "High order modulation in faster-than-Nyquist signaling communication systems," in *Proc. IEEE 80th Veh. Technol. Conf. (VTC-Fall)*, Vancouver, BC, Canada, Sep. 2014, pp. 1–5.
[183] L. Landau, M. Dorpinghaus, and G. P. Fettweis, "1-bit quantization and oversampling at the receiver: Communication over bandlimited channels with noise," *IEEE Commun. Lett.*, vol. 21, no. 5, pp. 1007–1010, May 2017.

[184] J. Wang, W. Tang, X. Li, and S. Li, "Filter hopping based faster-than-Nyquist signaling for physical layer security," *IEEE Wireless Commun. Lett.*, vol. 7, no. 6, pp. 894–897, Dec. 2018.
[185] S. Yuan, K. Igarashi, T. Tsuritani, and I. Morita, "Bit-error ratio performance improvement using iterative decoding for polybinary-shaped super-nyquist wavelength division multiplexed signals," *J. Lightw. Technol.*, vol. 35, no. 21, pp. 4605–4612, Nov. 1, 2017.
[186] Y. J. D. Kim and J. Bajcsy, "Binary faster than nyquist optical transmission via non-uniform power allocation," in *Proc. 13th Can. Workshop Inf. Theory*, Toronto, ON, Canada, Jun. 2013, pp. 180–185.
[187] L. Chen, J. Liu, and C. Guo, "Training aided frequency domain equalization with maximum-likelihood sequence detection in coherent optical communications systems using FTN signaling," in *Proc. 14th Int. Conf. Opt. Commun. Netw. (ICOCN)*, Nanjing, China, Jul. 2015, pp. 1–3.
[188] S. Zhang, D. Chang, O. A. Dobre, O. Omomukuyo, X. Lin, and R. Venkatesan, "Training symbol-based equalization for quadrature duobinary PDM-FTN systems," *IEEE Photon. Technol. Lett.*, vol. 29, no. 5, pp. 454–457, Mar. 1, 2017.
[189] M. Xiang, Z. Xing, E. El-Fiky, M. Morsy-Osman, Q. Zhuge, and D. V. Plant, "Single-lane 145 Gbit/s IM/DD transmission with faster-than-Nyquist PAM4 signaling," *IEEE Photon. Technol. Lett.*, vol. 30, no. 13, pp. 1238–1241, Jul. 1, 2018.
[190] H.-B. Zhang, N. Jiang, Z. Zheng, and W.-Q. Wang, "Experimental demonstration of FTN-NRZ, PAM-4, and duobinary based on 10-gbps optics in 100G-EPON," *IEEE Photon. J.*, vol. 10, no. 5, pp. 1–13, Oct. 2018.
[191] M. Guo, Y. Qiao, J. Zhou, X. Tang, J. Qi, S. Liu, X. Xu, and Y. Lu, "ICI cancellation based on MIMO decoding for FTN non-orthogonal FDM systems," *J. Lightw. Technol.*, vol. 37, no. 3, pp. 1045–1055, Feb. 1, 2019.
[192] J. Zhou, Y. Qiao, X. Huang, C. Yu, Q. Cheng, X. Tang, M. Guo, W. Liu, and Z. Li, "Joint FDE and MLSD algorithm for 56-Gbit/s optical FTN-PAM4 system using 10G-class optics," *J. Lightw. Technol.*, vol. 37, no. 13, pp. 3343–3350, Jul. 1, 2019.
[193] Z. Hu and C.-K. Chan, "A novel baseband faster-than-Nyquist non-orthogonal FDM IM/DD system with block segmented soft-decision decoder," *J. Lightw. Technol.*, vol. 38, no. 3, pp. 632–641, Feb. 1, 2020.
[194] N. Pham, J. B. Anderson, F. Rusek, J.-M. Freixe, and A. Bonnaud, "Exploring faster-than-Nyquist for satellite direct broadcasting," in *Proc. 31st AIAA Int. Commun. Satell. Syst. Conf.*, Florence, Italy, Oct. 2013, pp. 16–26.
[195] G. Maalouli and B. A. Bannister, "Performance analysis of a MMSE turbo equalizer with LDPC in a FTN channel with application to digital video broadcast," in *Proc. 48th Asilomar Conf. Signals, Syst. Comput.*, Pacific Grove, CA, USA, Nov. 2014, pp. 1871–1875.
[196] A. Abelló, D. Roque, J.-M. Freixe, and S. Mallier, "Faster-than-Nyquist signaling: On linear and non-linear reduced-complexity turbo equalization," *Anal. Integr. Circuits Signal Process.*, vol. 91, no. 2, pp. 267–276, May 2017.
[197] J.-A. Lucciardi, P. Potier, G. Buscarlet, F. Barrami, and G. Mesnager, "Non-linearized amplifier and advanced mitigation techniques: DVB-S2X spectral efficiency improvement," in *Proc. IEEE Global Commun. Conf. (GLOBECOM)*, Singapore, Dec. 2017, pp. 1–7.
[198] M. Maso and S. Tomasin, "Pre-equalized faster than nyquist transmission for 5G cellular microwave backhaul," in *Proc. IEEE 17th Int. Workshop Signal Process. Adv. Wireless Commun. (SPAWC)*, Edinburgh, U.K., Jul. 2016, pp. 1–6.
[199] Y.-J. Zhu, W.-Y. Wang, and G. Xin, "Faster-than-Nyquist signal design for multiuser multicell indoor visible light communications," *IEEE Photon. J.*, vol. 8, no. 1, pp. 1–12, Feb. 2016.
[200] J. Zhou, D. Li, and X. Wang, "Generalized faster-than-Nyquist signaling," in *Proc. IEEE Int. Symp. Inf. Theory (ISIT)*, Cambridge, MA, USA, Jul. 2012, pp. 1478–1482.
[201] M. El Hefnawy and H. Taoka, "Overview of faster-than-Nyquist for future mobile communication systems," in *Proc. IEEE 77th Veh. Technol. Conf. (VTC Spring)*, Dresden, Germany, Jun. 2013, pp. 1–5.
[202] D. Dasalukunte, V. Öwall, F. Rusek, and J. B. Anderson, *Faster Than Nyquist Signaling: Algorithms to Silicon*. Cham, Switzerland: Springer, 2014.
[203] J.-A. Lucciardi, N. Thomas, M.-L. Boucheret, C. Poulliat, and G. Mesnager, "Trade-off between spectral efficiency increase and PAPR reduction when using FTN signaling: Impact of non linearities," in *Proc. IEEE Int. Conf. Commun. (ICC)*, Kuala Lumpur, Malaysia, May 2016, pp. 1–7.
[204] D. Kang and W. Oh, "Faster than nyquist transmission with multiple turbo-like codes," *IEEE Commun. Lett.*, vol. 20, no. 9, pp. 1745–1747, Sep. 2016.
[205] C. Soltanpur and J. R. Cruz, "Uniformly oversampled sequence detection in the presence of unknown jitter," in *Proc. IEEE Int. Conf. Commun. (ICC)*, Paris, France, May 2017, pp. 1–6.
[206] Y. Zhu, M. Jiang, Z. Chen, and F. Zhang, "Terabit faster-than-Nyquist PDM 16-QAM WDM transmission with a net spectral efficiency of 7.96 b/s/Hz," *J. Lightw. Technol.*, vol. 36, no. 14, pp. 2912–2919, Jul. 15, 2018.

TAKUMI ISHIHARA (Member, IEEE) received the B.E., M.E., and Ph.D. degrees in computer and information sciences from the Tokyo University of Agriculture and Technology, Koganei, Japan, in 2016, 2017, and 2020, respectively. He is currently a Postdoctoral Research Fellow with the Institute of Industrial Science, The University of Tokyo, Tokyo, Japan. His research interest includes faster-than-Nyquist signaling. He was a recipient of the IEEE VTS Tokyo Chapter 2019 Young Researcher's Encouragement Award, the Yasujiro Niwa Outstanding Paper Award, in 2019, and the 33rd Telecom System Technology Award (Honorable Mention) from the Telecommunications Advancement Foundation, in 2018.

SHINYA SUGIURA (Senior Member, IEEE) received the B.S. and M.S. degrees in aeronautics and astronautics from Kyoto University, Kyoto, Japan, in 2002 and 2004, respectively, and the Ph.D. degree in electronics and electrical engineering from the University of Southampton, Southampton, U.K., in 2010. From 2004 to 2012, he was a Research Scientist with Toyota Central Research and Development Laboratories, Inc., Aichi, Japan. From 2013 to 2018, he was an Associate Professor with the Department of Computer and Information Sciences, Tokyo University of Agriculture and Technology, Tokyo, Japan. Since 2018, he has been an Associate Professor with the Institute of Industrial Science, The University of Tokyo, Tokyo, where he heads the Wireless Communications Research Group. He authored or coauthored over 80 IEEE journal articles. His research interests include wireless communications, networking, signal processing, and antenna technology.

LAJOS HANZO (Fellow, IEEE) received the D.Sc. degree from the University of Southampton, U.K., in 2004, and the Honorary Doctorate degrees from the Technical University of Budapest, in 2009, and The University of Edinburgh, in 2015. Over 40 of them are professors at various stages of their careers in academia and many of them are leading scientists in the wireless industry. He has published 1900+ contributions at IEEE Xplore and 19 Wiley-IEEE Press books. He has helped the fast-track career of 119 Ph.D. students. He is a Fellow of the REng, IET, and EURASIP. He is also a Foreign Member of the Hungarian Academy of Sciences and a former Editor-in-Chief of the IEEE Press. He has served as the Governor of both IEEE ComSoc and of VTS.